Anisotropic superfluidity of two-dimensional excitons in a periodic potential

Yu. E. Lozovik,[1,2] I. L. Kurbakov,[1] and Pavel A. Volkov[3]
[1]*Institute of Spectroscopy RAS, Moscow, Troitsk, Russia*
[2]*MIEM, National Research University Higher School of Economics, Moscow, Russia*
[3]*Theoretische Physik III, Ruhr-Universität Bochum, D-44780 Bochum, Germany*
(Received 7 December 2016; revised manuscript received 7 April 2017; published 27 June 2017)

We study anisotropies of the helicity modulus, excitation spectrum, sound velocity, and angle-resolved luminescence spectrum in a two-dimensional system of interacting excitons in a periodic potential. Analytical expressions for anisotropic corrections to the quantities characterizing superfluidity are obtained. We consider particularly the case of dipolar excitons in quantum wells. For GaAs/AlGaAs heterostructures as well as MoS_2/hBN/MoS_2 and $MoSe_2$/hBN/WSe_2 transition-metal dichalcogenide bilayers estimates of the magnitude of the predicted effects are given. We also present a method to control superfluid motion and to determine the helicity modulus in generic dipolar systems.

DOI: 10.1103/PhysRevB.95.245430

I. INTRODUCTION

Bose systems below quantum degeneracy temperature are extensively studied now both theoretically and experimentally. In the last decades many phenomena theoretically predicted for weakly interacting Bose gases (Bose-Einstein condensation (BEC), the Berezinskii-Kosterlitz-Thouless (BKT) transition [1] to the superfluid state in two-dimensional systems, and related effects) have been confirmed by experiments with ultracold atoms or molecules in optical or magnetic traps [2–5]. Actively studied are also the superfluidity and BEC in systems of excitons [6], bound states of an electron and a hole in semiconductor nanostructures, or exciton-polaritons, mixed states of an exciton and a photon in an optical cavity [7]. An important advantage of these systems over the atomic/molecular ones is the low effective mass of the particles, which leads to degeneracy temperatures on the order of 1 K for excitons and tens of K for exciton-polaritons compared to nK for the atomic systems. However, their drawback is the finite lifetime of the particles which makes the inclusion of kinetic effects in consideration necessary.

Systems of indirect, dipolar excitons are of particular interest. Their important virtue is the considerably long lifetime due to the small overlap of electron and hole wave functions which suppresses recombination. In contemporary studies the most widespread are 2D dipolar excitons [6,8,9] in coupled quantum wells (CQWs) [8] and wide single quantum wells (SQWs) [10,11] in a polarizing normal electric field. After a pump pulse creating 2D dipolar excitons in a QW they thermalize locally quite fast [12,13]. The excitons can then cool down to low temperatures [14] due to the interaction with the semiconductor lattice [15], as their lifetime is sufficiently long [10,16]. Disorder (due to impurities and interface roughness) [17,18], inevitably present in semiconductors, is screened by the interexcitonic interactions [19] and is usually weak in wide SQWs [10,20]. Fermionic (electron/hole) exchange effects in exciton-exciton interactions [21] which destroy the "Boseness" of excitons [22] and are disastrous [23–25] for the BEC are suppressed at low densities if the dipole-dipole interaction of excitons is sufficiently strong [26,27]. Excessive carriers [28] also suppressing BEC [29,30] can be compensated by injection of carriers with an opposite charge [10].

Finally, in the spatially separated [31,32] continuous wave pumping regime, cooled (charge compensated [33]) excitons flow to the studied area of the QW. They can be cooled additionally by evaporative techniques [34]. Due to the persistent inflow of cooled excitons even the degrees of freedom lowest in energy thermalize after a sufficiently long time [35]. These considerations show that the BEC [29] (or at least mesoscopic BEC [29] or quasicondensation [36]) of 2D dipolar excitons is experimentally feasible [6,37].

The remarkable experiments on exciton BEC have motivated rapid development of theoretical ideas [38]. Many interesting effects have been predicted for exciton BECs: the existence of nondissipative electric currents [39] and the internal Josephson effect [40], roton instability [41], autolocalization [42] and (mesoscopic [43]) supersolidity [44,45], BKT transition [46] (crossover [47]) and vortex formation [48], features of angle-resolved photoluminescence [49] and nonlinear optical phenomena [50], as well as topological excitons [51], dipole superconductivity [52], and the Casimir effect [53]. Another interesting topic is exciton spin effects that have been predicted to lead to a multicomponent BEC [22], which has been recently observed experimentally [54].

Important progress has been also achieved for other realizations: electron-electron bilayers in a quantizing magnetic field [55], graphene bilayers [56] (including realizations with a band gap [57]), topological insulator films [58], and cyclotron spin-flip excitons in wide GaAs single quantum wells with a 2D quantum Hall electron gas at a filling factor of $\nu = 2$ [59].

A high-temperature BEC phase of excitons [60] can occur in 2D transition-metal dichalcogenides [61] based on [62,63] $MoSe_2$-WSe_2 or [64] MoS_2-MoS_2 bilayers if an hBN film is sandwiched in between two monolayers of a bilayer [60].

Various types of electrostatic [65,66] and other [31,67] traps for excitons are analogous to laser and magnetic traps for the atomic ensembles, e.g., flat traps [68] where during exciton lifetime an equilibrium density profile of excitons is formed [69]. Specially designed electrostatic [70,71] and magnetic [72] lattices allow one to create an external periodic potential for excitons. Application of various voltage patterns [73] can be used to create different types of potentials: confining [65], random one-dimensional, and dividing the system with

a barrier [74]. Superimposing two striped patterns [75] or using more complex structures [71] allows one to construct 2D potentials of various forms for excitons. Varying the in-plane landscape of an electrode [66] allows one to create potentials [76] and traps [77] of different types as well as potential energy gradients [78]. There is also another method of controlling excitons: creating deformation waves [79]. A stationary periodic potential in this case can be realized with a standing acoustic wave.

BEC and superfluidity in periodic potentials is actively investigated for bosonic atoms. Considerable success in this field has been attained with atomic systems in laser traps [81]: excitation spectrum measurements by Bragg spectroscopy were performed [82], a roton-maxon form of the excitation spectrum has been demonstrated [83], processes similar to Bloch oscillations in crystals have been observed [84]. From the theory side the ground state and excitation spectrum have been calculated for models with a one-dimensional periodic potential [85] and effects similar to the ones for electrons in a crystal have been predicted, such as Bloch oscillations [86]. The formation of new phases by spontaneous symmetry breaking is also studied, in particular for dipole-type interacting systems [87,88].

The majority of works, however, rely on the Bose-Hubbard model corresponding to a very strong periodic potential. This regime is hardly attainable for excitons for the following reasons. In the deep-modulation regime, the effective exciton mass is exponentially large [89]. Consequently, the superfluid transition temperature is exponentially low, and even more importantly, the sensitivity to disorder [90,91] and free carriers increases greatly, setting very stringent constraints on the sample quality.

We consider thus the experimentally relevant case of excitons in a *weak* periodic potential which is opposed to the Bose-Hubbard approximation. For a macroscopically ordered excitonic system in the weak-modulation regime we show that *anisotropic superfluidity* takes place, i.e., the dependence of the superfluid system observables on the direction in space. The superfluid density in this case turns out to be a tensor instead of a scalar. This precludes an interpretation of the superfluid density as being proportional to the number of particles in the condensate, which is always a scalar [92].

One of the most famous examples of an anisotropic superfluid system is liquid ^{3}He [93–95]. Anisotropy there is caused by a condensate of atomic pairs with nonzero spin formed at low temperatures. Anisotropic superfluidity has been observed in atomic systems in optical lattices [96,97] due to asymmetry $x \leftrightarrow y$ of the lattice potential. In this case anisotropy can be controlled: the reciprocal lattice vector sets the selected direction and the amplitude of the potential governs the strength of anisotropic effects.

There are the following observable effects related to anisotropic superfluidity:

(1) Changes in the vortex shape: nondissipative currents around the vortex core flow in ellipses rather than circles. In the 3D case this leads to an elliptical form of vortex loops [97]. Vortex cores become elliptical as well [98].

(2) Anisotropic optical coherence due to anisotropy of correlations [99]: visibility of the interference pattern in Young's experiment [29] depends on the mutual orientation of the condensate areas emitting light [100]. In particular, coherence length may depend on the direction in space [80].

(3) In the strong-anisotropy limit a finite system can effectively change its dimensionality [101]. Thus a long quasi-1D strip can behave like a 2D system [96] so that its transition to the normal phase can be of BKT type. In 3D systems vortex loops can collapse to 2D vortex-antivortex pairs, dissociation of which leads to a BKT-type transition [97,102].

(4) Finally, let us mention effects caused by the anisotropy of interparticle interactions rather than the superfluid density: anisotropies of sound [103], Landau critical velocity [104], dissipation [105], and of vortex properties: shape of the vortex core and intervortex interactions [106], as well as appearance of complex vortex structures [107].

The aim of our work is to demonstrate the anisotropic superfluidity in a model of a weakly interacting two-dimensional Bose gas in a periodic potential, namely the effect of anisotropy of the potential on the superfluid motion characteristics and the elementary excitations. We will concentrate our attention on the dynamical/superfluid properties, and their anisotropic character. In the present article we consider a system of 2D dipolar excitons as an experimental realization of the model studied, though qualitative conclusions can be generalized to ultracold atomic systems. We present estimates of the magnitudes of the effects related to anisotropic superfluidity for the chosen physical realization.

The article is organized as follows. In Sec. II the tensor character of the superfluid density and anisotropic effects are discussed qualitatively. In Sec. III a theoretical model is considered and analytical expressions for observable quantities are obtained. In Sec. IV physical realizations of the studied model are described and qualitative manifestations of the anisotropic superfluidity are discussed. In Sec. V we present estimates for the experimental effects proposed. An outlook of the results obtained is presented in Sec. VI.

II. ANISOTROPIC SUPERFLUIDITY

In this work we consider three types of anisotropy: of sound velocity C_s and of quantities related to linear response—superfluid mass density ρ_s and helicity modulus Υ_s [108]. Anisotropy can have effect not on all the quantities; e.g., for bosons with an anisotropic interaction the critical velocity turns out to be anisotropic while the sound velocity is not [104].

Quantity C_s can be deduced from the single-particle excitation spectrum $\varepsilon(\mathbf{p})$ of the system. In the isotropic case energy of the excitations depends only on magnitude of the vector $\mathbf{p}$; we will show that in the presence of an anisotropic potential the excitation spectrum as well as C_s also depend on the direction of $\mathbf{p}$. A direct measurement of C_s or $\varepsilon(\mathbf{p})$ is needed to detect this type of anisotropy.

Quantities ρ_s and Υ_s are linear response coefficients connecting macroscopic flow parameters of the system such as current $\mathfrak{J}$, total momentum $\mathfrak{P}$, and energy E to infinitesimal probe velocity $\mathbf{v}$ or momentum $\mathbf{P}$ transferred to each particle.

In the isotropic case one has

$$\frac{\mathfrak{J}}{S} = \frac{\hbar}{2miS}\int \langle \hat{\Psi}^+(\mathbf{r})\nabla\hat{\Psi}(\mathbf{r}) - [\nabla\hat{\Psi}^+(\mathbf{r})]\hat{\Psi}(\mathbf{r})\rangle d\mathbf{r} = \mathrm{Y}_s\mathbf{P},$$
$$\frac{\mathfrak{P}}{S} = \frac{1}{S}\int \langle \hat{\Psi}^+(\mathbf{r})(-i\hbar\nabla)\hat{\Psi}(\mathbf{r})\rangle d\mathbf{r} = \rho_s\mathbf{v}, \quad (1)$$
$$\frac{E}{S} = \frac{E(\mathbf{P}=0)}{S} + \frac{\mathrm{Y}_s\mathbf{P}^2}{2} = \frac{E(\mathbf{P}=0)}{S} + \frac{\rho_s\mathbf{v}^2}{2},$$

where S is the system's area, $\mathbf{P} = m\mathbf{v}$ is the probe momentum, and a "phase twist" [108] condition is implied onto the field operator $\hat{\Psi}(\mathbf{r})$: $\hat{\Psi}(\mathbf{r}+\mathbf{L}) = \exp(iPL/\hbar)\hat{\Psi}(\mathbf{r})$, where L is the linear size of the system. It is natural to assume that definitions of ρ_s and Y_s through momentum/current and energy coincide, though a general proof (including anisotropic case) for this statement has not been found by the authors but for the model we consider it follows from direct verification of the relation $\mathfrak{J} = dE/d\mathbf{P}$.

Quantities ρ_s and Y_s can be presented in the following form: $\rho_s = n_s m$ and $\mathrm{Y}_s = n_s/m$, where m is the mass of particles and n_s is the superfluid density. Temperature and *external fields* can lead to n_s being smaller than full density n. This effect can be interpreted as being due to presence of a "normal component," which can be subject to dissipation and does not take part in the superfluid motion.

Let us discuss qualitatively what differences will be there for a system in an anisotropic external potential. For a single-particle problem it is known that a periodic potential leads to a change of the initial particle's mass to an effective mass tensor. Noticing that ρ_s and Y_s play a role similar to mass in the expression for energy of the multiparticle system (coefficient with the square of velocity/momentum) we assume that ρ_s and Y_s are also anisotropic tensor quantities. In this case for infinitesimal $\mathbf{P}$, $\mathbf{v}$ energy of the system per unit area will have the form

$$\left.\frac{E}{S}\right|_{\mathbf{P}\to 0} \approx \frac{E(\mathbf{P}=0)}{S} + \sum_{ij}\frac{(\rho_s)_{ij}v_i v_j}{2} = \frac{E(\mathbf{P}=0)}{S} + \sum_{ij}\frac{(\mathrm{Y}_s)_{ij}P_i P_j}{2}, \quad (2)$$

or after substitution $P_1 = |\mathbf{P}|\cos\phi$, $P_2 = |\mathbf{P}|\sin\phi$:

$$\left.\frac{E}{S}\right|_{\mathbf{P}\to 0} \approx \frac{E(\mathbf{P}=0)}{S} + \frac{\mathrm{Y}_s(\phi)\mathbf{P}^2}{2}. \quad (3)$$

Total momentum $\mathfrak{P}$ and current $\mathfrak{J}$ will be related to probe momentum and velocity in a similar way:

$$\frac{\mathfrak{J}_i}{S} = \sum_j (\mathrm{Y}_s)_{ij}P_j,$$
$$\frac{\mathfrak{P}_i}{S} = \sum_j (\rho_s)_{ij}v_j. \quad (4)$$

In particular, it follows from (4) that the probe velocity can be noncollinear with the total momentum. Quantity n_s can be defined similarly to the isotropic case $\rho_{jl} = m^2\mathrm{Y}^{jl} = mn_s^{jl}$; however, it will also be a tensor quantity which complicates the usual interpretation of the system as a mixture of "normal" and "superfluid" components. Let us mention that in the case when the initial mass of the particles is taken to be anisotropic (e.g., for a semiconductor with noncubic lattice) n_s can be a nonsymmetric tensor unlike ρ_s and Y_s for which symmetry follows from the definition (2).

Let us discuss methods to measure the helicity modulus and superfluid mass density experimentally. To determine them one should transfer a uniform momentum $\mathbf{P}$ or velocity $\mathbf{v}$ to all the particles. Both options can be implemented: momentum can be transferred to excitons in crossed magnetic and electric fields by an adiabatic switch of the last one (see Sec. IV) and velocity, by setting the external potential into motion $V(\mathbf{r}) \to V(\mathbf{r}-\mathbf{v}t)$. In the first case there will also be an effective addition to the exciton mass although it is negligibly small in sufficiently weak magnetic fields. Transforming the Hamiltonian to a moving reference frame one can show the equivalence of these approaches and that the transferred momentum is related to velocity through $\mathbf{P} = m\mathbf{v}$, where m is the exciton mass. What is left is to propose a method of measuring the system's current and momentum which is done in Sec. IV for a dipolar excitonic system.

Concluding the above one can see that to determine the parameters of anisotropic superfluidity one has to find mean values of Hamiltonian $\langle\hat{H}\rangle$ and current or momentum for the system in a state corresponding to a uniform motion with single-particle momentum $\mathbf{P}$ or velocity $\mathbf{v}$ and also the excitation spectrum $\varepsilon(\mathbf{p})$.

III. THEORETICAL ANALYSIS

Let us proceed to the theoretical model formulation. We will work with the following assumptions:

(1) The density of excitons is low enough and repulsion between the particles is sufficiently strong so that their composite fermionic structure can be ignored. Therefore, the excitons are considered to be strictly bosons.

(2) Correlations are weak so that $(N-N_0)/N \ll 1$, where N is the total number of particles and N_0 is the number of particles in the condensate [109].

(3) Modulation of the condensate profile by the periodic external field is weak. Specifically, we assume that V_0 is small compared to μ.

(4) Interparticle interactions do not involve spin and thus we ignore spin degrees of freedom for excitons [110].

Thus, the considered system is a gas of weakly interacting bosons in an external periodic potential. The Hamiltonian of the system (after change of variables from particle number to the chemical potential μ) is

$$\hat{H} - \mu\hat{N} = \int \hat{\Psi}^+(\mathbf{r})\left(-\frac{\hbar^2}{2m}\Delta + V(\mathbf{r}) - \mu\right)\hat{\Psi}(\mathbf{r})d\mathbf{r} + \frac{1}{2}\int \hat{\Psi}^+(\mathbf{r})\hat{\Psi}^+(\mathbf{r}')U(\mathbf{r}-\mathbf{r}')\hat{\Psi}(\mathbf{r}')\hat{\Psi}(\mathbf{r})d\mathbf{r}'d\mathbf{r}, \quad (5)$$

where $V(\mathbf{r}) = V_0\cos\mathbf{qr}$ is the external potential and $U(\mathbf{r}-\mathbf{r}')$ is the interparticle potential, which we consider to be symmetric under transformation $\mathbf{r} \leftrightarrow \mathbf{r}'$. We also assume the initial mass of the particles to be isotropic (it is true for, e.g., excitons in GaAs-based structures). In what follows we will consider the system at $T = 0$.

For weakly correlated 2D bosons a standard Bogoliubov approach is applicable, provided one replaces bare interaction with an effective one arising from the summation of ladder diagrams [111]. The condensate contribution to the energy of the system is

$$E_{\rm cond} = \int \Phi^*(\mathbf{r})\left(-\frac{\hbar^2}{2m}\Delta + V(\mathbf{r})\right)\Phi(\mathbf{r})d\mathbf{r} + \frac{1}{2}\int \Phi^*(\mathbf{r})\Phi^*(\mathbf{r}')U(\mathbf{r}-\mathbf{r}')\Phi(\mathbf{r})\Phi(\mathbf{r}')d\mathbf{r}'d\mathbf{r}. \quad (6)$$

Condensate wave function $\Phi(\mathbf{r})$ satisfies the Gross-Pitaevskii equation (with μ being determined by normalization condition):

$$\left(-\frac{\hbar^2}{2m}\Delta + V(\mathbf{r}) - \mu + \int U(\mathbf{r}-\mathbf{r}')|\Phi(\mathbf{r}')|^2 d\mathbf{r}'\right)\Phi(\mathbf{r}) = 0,$$
$$\int |\Phi(\mathbf{r})|^2 d\mathbf{r} = N_0. \quad (7)$$

One should keep in mind that N is the problem parameter while N_0 is not. They are connected through the relation $N = N_0 + N'$, where N' is the number of particles depleted from the condensate which will be defined later in the article; both N_0 and N' can depend on $\mathbf{P}$. We seek the solutions of Eq. (7) as a power series in V_0. For a uniformly moving condensate the zeroth-order solution is taken as constant $\times\, e^{i\mathbf{kr}}$, where $\mathbf{k} = \mathbf{P}/\hbar$. The solution for $\Phi(\mathbf{r})$ and μ up to the second order in V_0 is

$$\Phi(\mathbf{r}) \approx \sqrt{n_0}e^{i\mathbf{kr}} \times \left[\left(1 - V_0^2\Delta\Phi_0\right) - V_0\Phi_+ e^{i\mathbf{qr}} - V_0\Phi_- e^{-i\mathbf{qr}}\right],$$
$$\Phi_\pm = \frac{T \mp \alpha}{2\kappa}, \quad \Delta\Phi_0 = \frac{\Phi_+^2 + \Phi_-^2}{2},$$
$$\mu = \frac{\hbar^2\mathbf{k}^2}{2m} + n_0U_0 - V_0^2T\frac{T^2-\alpha^2}{2\kappa^2}, \quad (8)$$

where notations are introduced as follows: $n_0 = N_0/S$, $U_\mathbf{q} = \int U(\mathbf{r})e^{i\mathbf{qr}}d\mathbf{r}$, $U = n_0U_\mathbf{q}$, $T = \hbar^2\mathbf{q}^2/2m$, $\alpha = \hbar\mathbf{qP}/m$, $\kappa = T^2 + 2TU - \alpha^2$. We have omitted the terms $\sim e^{2i\mathbf{qr}}$, $e^{-2i\mathbf{qr}}$ as their contribution to the quantities calculated further in text (condensate energy, excitation spectrum, etc.) is of higher than second order in V_0. In the case $\mathbf{P} = 0$ the solution takes the form

$$\Phi(\mathbf{r}) \approx \sqrt{n_0}\left(1 - \frac{V_0^2}{4(T+2U)^2} - \frac{V_0}{T+2U}\cdot\cos\mathbf{qr}\right), \quad (9)$$

which clearly demonstrates periodic modulations of the condensate's density (with period determined by the external potential), i.e., diagonal long-range order.

In Fig. 1 we compare the approximate solution (9) with a full numerical solution. The approximation (9) gives a reasonably good result (average relative error <10%), particularly taking into account rather large anisotropic effects (see Table II) for the same set of parameters. In what follows we use (8) to obtain closed analytical expressions for the quantities of interest.

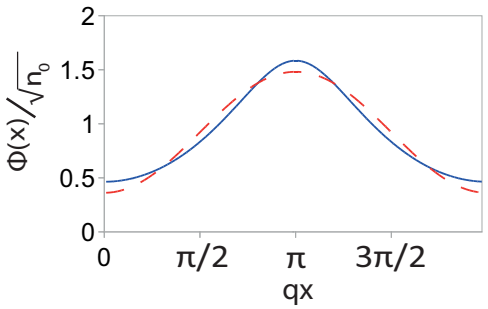

FIG. 1. Solution of the Gross-Pitaevskii equation (7) with the parameters taken for the MoS_2/hBN/MoS_2 structure (see Table I). Red dashed line is the approximate solution (9); solid blue line is the numerical solution of (7).

Substituting the obtained solution into the expression for the energy (6) one has

$$\frac{E_{\rm cond}}{S} = \frac{E_{\rm cond}(\mathbf{P}=0)}{S} + \frac{\mathbf{P}^2}{2m}n_0 + \frac{1}{2}\left[n_0^2 - n_0^2(\mathbf{P}=0)\right]U_0 - \frac{mV_0^2n_0\alpha^2}{\hbar^2\mathbf{q}^2(T+2U)^2}. \quad (10)$$

It is also possible to calculate the condensate contribution to the current $\mathfrak{J}$:

$$\frac{\mathfrak{J}_{\rm cond}}{S} = \frac{\mathbf{P}}{m}n_0 - \frac{V_0^2n_0\alpha\hbar\mathbf{q}}{mT(T+2U)^2}. \quad (11)$$

Let us move on to the noncondensate part. We use the Bogoliubov transformation:

$$\hat{\Psi}'(\mathbf{r}) = \sum_l [u_l(\mathbf{r})\hat{a}_l - v_l^*(\mathbf{r})\hat{a}_l^+], \quad (12)$$

where operators $\hat{a}_l$ and $\hat{a}_l^+$ satisfy Bose commutation relations. Diagonalizing the noncondensate Hamiltonian we obtain equations for $u_l(\mathbf{r})$ and $v_l(\mathbf{r})$:

$$\tilde{T}u_l(\mathbf{r}) - \tilde{U}v_l(\mathbf{r}) = \varepsilon_l u_l(\mathbf{r}),$$
$$\tilde{T}v_l^*(\mathbf{r}) - \tilde{U}u_l^*(\mathbf{r}) = -\varepsilon_l v_l^*(\mathbf{r}), \quad (13)$$

where

$$\tilde{T}f(\mathbf{r}) \equiv \left(-\frac{\hbar^2}{2m}\Delta + V(\mathbf{r}) - \mu + \int |\Phi(\mathbf{r}')|^2U(\mathbf{r}-\mathbf{r}')d\mathbf{r}'\right)f(\mathbf{r}) + \Phi(\mathbf{r})\int \Phi^*(\mathbf{r}')U(\mathbf{r}-\mathbf{r}')f(\mathbf{r}')d\mathbf{r}',$$
$$\tilde{U}f(\mathbf{r}) \equiv \Phi(\mathbf{r})\int \Phi(\mathbf{r}')U(\mathbf{r}-\mathbf{r}')f(\mathbf{r}')d\mathbf{r}'.$$

One can show that if the above equations are satisfied then the excitation Hamiltonian takes the form

$$(\hat{H} - \mu\hat{N})' = \sum_l \varepsilon_l\hat{a}_l^+\hat{a}_l - \sum_l \varepsilon_l\int |v_l(\mathbf{r})|^2 d\mathbf{r},$$

and the mean noncondensate density is

$$n' = \frac{1}{S}\int \langle \hat{\Psi}'^{+}(\mathbf{r})\hat{\Psi}'(\mathbf{r})\rangle d\mathbf{r} = \frac{1}{S}\int \sum_{l} |v_l(\mathbf{r})|^2 d\mathbf{r}.$$

Equations (13) are solved (and the excitation spectrum is found) approximately up to the second order in V_0. The Bogoliubov coefficients u, v are then

$$\begin{aligned}
u_l(\mathbf{r}) &= \frac{1}{\sqrt{S}} u_{\mathbf{p}} e^{i(\mathbf{k}+\mathbf{p})\mathbf{r}},\ v_l(\mathbf{r}) = \frac{1}{\sqrt{S}} v_{\mathbf{p}} e^{i(-\mathbf{k}+\mathbf{p})\mathbf{r}},\\
u_{\mathbf{p}} &= u^0_{\mathbf{p}} - V_0(u^+_{\mathbf{p}} e^{i\mathbf{q}\mathbf{r}} + u^-_{\mathbf{p}} e^{-i\mathbf{q}\mathbf{r}}) + V_0^2 \Delta u_0,\\
v_{\mathbf{p}} &= v^0_{\mathbf{p}} - V_0(v^+_{\mathbf{p}} e^{i\mathbf{q}\mathbf{r}} + v^-_{\mathbf{p}} e^{-i\mathbf{q}\mathbf{r}}) + V_0^2 \Delta v_0,\\
u^0_{\mathbf{p}} &= \frac{1}{2}\left(\sqrt{\frac{2m\varepsilon^0_{\mathbf{p}}}{\hbar^2\mathbf{p}^2}} + \sqrt{\frac{\hbar^2\mathbf{p}^2}{2m\varepsilon^0_{\mathbf{p}}}}\right), v^0_{\mathbf{p}} = \frac{1}{2}\left(\sqrt{\frac{2m\varepsilon^0_{\mathbf{p}}}{\hbar^2\mathbf{p}^2}} - \sqrt{\frac{\hbar^2\mathbf{p}^2}{2m\varepsilon^0_{\mathbf{p}}}}\right),\\
\varepsilon^0_{\mathbf{p}} &= \sqrt{\left(\frac{\hbar^2\mathbf{p}^2}{2m}\right)^2 + n_0 U_{\mathbf{p}} \frac{\hbar^2\mathbf{p}^2}{m}},
\end{aligned} \tag{14}$$

where $v^{\pm}_{\mathbf{p}}$ and $u^{\pm}_{\mathbf{p}}$ are given by

$$\begin{aligned}
u^{\pm}_{\mathbf{p}} &= \frac{A_{\pm}\left(T_{\pm} + n_0 U_{\mathbf{p}\pm\mathbf{q}} + \varepsilon^0_{\mathbf{p}} \mp \alpha\right) + B_{\pm} n_0 U_{\mathbf{p}\pm\mathbf{q}}}{\left(\varepsilon^0_{\mathbf{p}\pm\mathbf{q}}\right)^2 - \left(\varepsilon^0_{\mathbf{p}} \mp \alpha\right)^2},\\
v^{\pm}_{\mathbf{p}} &= \frac{A_{\pm} n_0 U_{\mathbf{p}\pm\mathbf{q}} + B_{\pm}\left(T_{\pm} + n_0 U_{\mathbf{p}\pm\mathbf{q}} - \varepsilon^0_{\mathbf{p}} \pm \alpha\right)}{\left(\varepsilon^0_{\mathbf{p}\pm\mathbf{q}}\right)^2 - \left(\varepsilon^0_{\mathbf{p}} \mp \alpha\right)^2},\\
A_{\pm} &= u^0_{\mathbf{p}} \frac{T^2 - \alpha^2}{2\kappa} - \frac{T n_0 (U_{\mathbf{p}} + U_{\mathbf{p}\pm\mathbf{q}})}{2\kappa} f_- \pm \alpha n_0 \frac{U_{\mathbf{p}} f_- - U_{\mathbf{p}\pm\mathbf{q}} f_+}{2\kappa},\\
B_{\pm} &= v^0_{\mathbf{p}} \frac{T^2 - \alpha^2}{2\kappa} + \frac{T n_0 (U_{\mathbf{p}} + U_{\mathbf{p}\pm\mathbf{q}})}{2\kappa} f_- \pm \alpha n_0 \frac{U_{\mathbf{p}} f_- + U_{\mathbf{p}\pm\mathbf{q}} f_+}{2\kappa},\\
f_+ &= \sqrt{\frac{2m\varepsilon^0_{\mathbf{p}}}{\hbar^2\mathbf{p}^2}},\ f_- = \sqrt{\frac{\hbar^2\mathbf{p}^2}{2m\varepsilon^0_{\mathbf{p}}}},
\end{aligned} \tag{15}$$

where $T_{\pm} = \hbar^2(\mathbf{p} \pm \mathbf{q})^2/2m$. The second-order corrections $\Delta v^0_{\mathbf{p}}$ and $\Delta u^0_{\mathbf{p}}$ are

$$\begin{aligned}
2v^0_{\mathbf{p}}\Delta v^0_{\mathbf{p}} &= \frac{n_0 U_{\mathbf{p}}}{2\left(\varepsilon^0_{\mathbf{p}}\right)^2}\left(A v^0_{\mathbf{p}} + B u^0_{\mathbf{p}}\right) + C\left(v^0_{\mathbf{p}}\right)^2,\\
2u^0_{\mathbf{p}}\Delta u^0_{\mathbf{p}} &= \frac{n_0 U_{\mathbf{p}}}{2\left(\varepsilon^0_{\mathbf{p}}\right)^2}\left(A v^0_{\mathbf{p}} + B u^0_{\mathbf{p}}\right) + C\left(u^0_{\mathbf{p}}\right)^2,\\
A &= \frac{T^2 - \alpha^2}{2\kappa}(u^+_{\mathbf{p}} + u^-_{\mathbf{p}}) - \frac{T^2 - \alpha^2}{2\kappa^2} T u^0_{\mathbf{p}} + n_0 U_{\mathbf{p}}[(\Phi^2_+ + \Phi^2_-) f_- + \Phi_+ v^-_{\mathbf{p}} + \Phi_- v^+_{\mathbf{p}} - \Phi_+ u^+_{\mathbf{p}} - \Phi_- u^-_{\mathbf{p}}]\\
&\quad + n_0 U_{\mathbf{p}+\mathbf{q}} \Phi_-\left(\Phi_+ v^0_{\mathbf{p}} - \Phi_- u^0_{\mathbf{p}} + v^+_{\mathbf{p}} - u^+_{\mathbf{p}}\right) + n_0 U_{\mathbf{p}-\mathbf{q}} \Phi_+\left(\Phi_- v^0_{\mathbf{p}} - \Phi_+ u^0_{\mathbf{p}} + v^-_{\mathbf{p}} - u^-_{\mathbf{p}}\right),\\
B &= \frac{T^2 - \alpha^2}{2\kappa}(v^+_{\mathbf{p}} + v^-_{\mathbf{p}}) - \frac{T^2 - \alpha^2}{2\kappa^2} T v^0_{\mathbf{p}} + n_0 U_{\mathbf{p}}[-(\Phi^2_+ + \Phi^2_-) f_- + \Phi_+ u^+_{\mathbf{p}} + \Phi_- u^-_{\mathbf{p}} - \Phi_+ v^-_{\mathbf{p}} - \Phi_- v^+_{\mathbf{p}}]\\
&\quad + n_0 U_{\mathbf{p}+\mathbf{q}} \Phi_+\left(\Phi_- u^0_{\mathbf{p}} - \Phi_+ v^0_{\mathbf{p}} + u^+_{\mathbf{p}} - v^+_{\mathbf{p}}\right) + n_0 U_{\mathbf{p}-\mathbf{q}} \Phi_-\left(\Phi_+ u^0_{\mathbf{p}} - \Phi_- v^0_{\mathbf{p}} + u^-_{\mathbf{p}} - v^-_{\mathbf{p}}\right),\\
C &= (v^+_{\mathbf{p}} + u^+_{\mathbf{p}})(v^+_{\mathbf{p}} - u^+_{\mathbf{p}}) + (v^-_{\mathbf{p}} + u^-_{\mathbf{p}})(v^-_{\mathbf{p}} - u^-_{\mathbf{p}}).
\end{aligned} \tag{16}$$

The excitation spectrum is given by

$$\begin{aligned}
\varepsilon_{\mathbf{p}} &= \varepsilon^0_{\mathbf{p}} + \hbar\mathbf{p}\frac{\mathbf{P}}{m} + V_0^2 \Delta\varepsilon_{\mathbf{p}},\\
\Delta\varepsilon_{\mathbf{p}} &= -\left(u^0_{\mathbf{p}} A + v^0_{\mathbf{p}} B\right).
\end{aligned} \tag{17}$$

In Fig. 2 we present a spectrum for one of the structures described in Secs. IV and V. At low $\mathbf{p}$ it has the linear Bogoliubov form with anisotropic sound velocities (see also Table II). For $\mathbf{p} \parallel \mathbf{q}$ one can see a characteristic flattening starting near $p \approx q/2$. This

is a signature of the spectrum splitting near the edge of the Brillouin zone defined by the external potential. The expression (17) is not applicable in this region. In what follows we consider the superfluid properties of the system, which are determined by the low-$\mathbf{p}$ part of the spectrum, so we do not consider the effects induced by the splitting and the corresponding region is omitted in the figure. Another interesting detail is a developing roton-minimum-like feature for $\mathbf{p} \perp \mathbf{q}$. However, it is clearly far from an instability and we do not study this feature in detail, as it does not affect the superfluid properties that we consider below.

For the depleted density we have

$$n' = n - n_0 = \frac{1}{(2\pi)^2}\int d\mathbf{p}\{|v_{\mathbf{p}}^0|^2 + V_0^2|v_{\mathbf{p}}^+|^2 + V_0^2|v_{\mathbf{p}}^-|^2 + 2V_0^2 v_{\mathbf{p}}^0 \Delta v_{\mathbf{p}}^0\}$$
$$= \frac{1}{(2\pi)^2}\int d\mathbf{p}\left\{|v_{\mathbf{p}}^0|^2 + V_0^2 n_0 U_{\mathbf{p}} \frac{A v_{\mathbf{p}}^0 + B u_{\mathbf{p}}^0}{2\left(\varepsilon_{\mathbf{p}}^0\right)^2} + V_0^2(|v_{\mathbf{p}}^+|^2 + |v_{\mathbf{p}}^-|^2)u_0^2(\mathbf{p}) - V_0^2(|u_{\mathbf{p}}^+|^2 + |u_{\mathbf{p}}^-|^2)v_0^2(\mathbf{p})\right\}. \quad (18)$$

Thus, taking into account $N_0 + N' = N$ we have an equation for N_0. For an arbitrary potential the integral in (18) cannot be evaluated analytically; however, one can study its convergence. For convergence at $\mathbf{p} \to 0$ and $\mathbf{p} \to \infty$ it is sufficient for the potential $U_{\mathbf{p}}$ to be finite. In the second order in V_0 there are also two problematic points where $\varepsilon_{\mathbf{p}} = \varepsilon_{\mathbf{p}+\mathbf{q}} \mp \alpha$. For $\mathbf{P} = 0$ ($\alpha = 0$) the singularity can be integrated in the principal value sense without taking splitting into account. In the case when $\mathbf{P} \neq 0$ this is not possible because the singularity is $1/x^2$. However, taking splitting into account will certainly lead to a finite result. Then it turns out that condensate depletion in the system is finite and consequently there is a nonzero condensate fraction for the weakly correlated system [112].

The contribution of the depleted particles to the energy of the system takes the form

$$\langle \hat{H}' \rangle = \mu N' - \sum_l \varepsilon_l \int |v_l(\mathbf{r})|^2 d\mathbf{r}$$
$$= \mu n' S - \frac{S}{(2\pi)^2}\int d\mathbf{p}\varepsilon(\mathbf{p})\left\{|v_{\mathbf{p}}^0|^2 + V_0^2 n_0 U_{\mathbf{p}} \frac{A v_{\mathbf{p}}^0 + B u_{\mathbf{p}}^0}{2\left(\varepsilon_{\mathbf{p}}^0\right)^2}\right.$$
$$\left. + V_0^2(|v_{\mathbf{p}}^+|^2 + |v_{\mathbf{p}}^-|^2)\left(u_{\mathbf{p}}^0\right)^2 - V_0^2(|u_{\mathbf{p}}^+|^2 + |u_{\mathbf{p}}^-|^2)\left(v_{\mathbf{p}}^0\right)^2\right\}. \quad (19)$$

Let us discuss the convergence of expression (19). The first term diverges at large momenta for potentials finite at $\mathbf{p} \to \infty$; however, this is resolved by taking the second Born approximation for the interaction potential into account. For convergence of the remaining terms at $\mathbf{p} \to \infty$ it is necessary to put a more stringent condition than before on $U_{\mathbf{p}}$: $2U_{\mathbf{p}} - U_{\mathbf{p}+\mathbf{q}} - U_{\mathbf{p}-\mathbf{q}} = O(\frac{1}{|\mathbf{p}|^\beta})$, $\beta > 0$, $|\mathbf{p}| \to \infty$. However, even for a delta-function potential it is clearly fulfilled. For real physical potentials this condition is met because of the finite size of the particles, inside which large repulsion forces act, e.g., in a model potential for dipolar excitons constructed in accord with the results of a numerical simulation (see Appendix A 1).

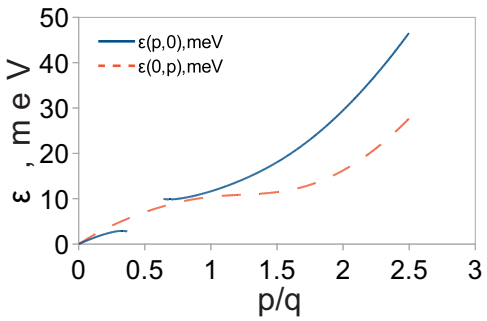

FIG. 2. Spectrum of elementary excitations [Eq. (17)] for the MoS_2/hBN/MoS_2 structure (see Table I). Shown are the excitation energies depending on the value of the momentum $\mathbf{p}$ measured in units of the reciprocal vector of the periodic potential $\mathbf{q}$ for $\mathbf{p}$ along and across $\mathbf{q}$. For $\mathbf{p} \parallel \mathbf{q}$ the region where the splitting effects become important (see text) is omitted.

It is also not possible to give an analytical answer for (19) in the general case but it is possible to draw conclusions on the dependence of $\langle \hat{H}' \rangle$ on $\mathbf{P}$. It turns out [113] that for small $\mathbf{P}$

$$\langle \hat{H}' \rangle \approx \langle \hat{H}' \rangle\,|_{\mathbf{P}\to 0} + a_{E'}\alpha^2,$$
$$n' \approx n'\,|_{\mathbf{P}\to 0} + a_{n'}\alpha^2, \quad (20)$$

where $a_{E'}$ and $a_{n'}$ are constants. Now one can show using the expression (10) that the total energy of the system takes the form

$$\left.\frac{E}{S}\right|_{\mathbf{P}\to 0} \approx \frac{E(\mathbf{P}=0)}{S} + \frac{\mathbf{P}^2}{2m}n + \frac{a_E}{2}(\mathbf{qP})^2$$
$$= \frac{E(\mathbf{P}=0)}{S} + \sum_{ij}\left(\frac{n}{m}\delta_{ij} + a_E q_i q_j\right)P_i P_j/2, \quad (21)$$

where a_E is a constant. Comparing with helicity modulus definition (2) we have $(\Upsilon_s)_{ij} = (n_0/m\delta_{ij} + a_E q_i q_j)$. To obtain superfluid mass density ρ_s one should express momentum $\mathbf{P}$ through velocity and substitute into (21). Comparing with the definition we have $(\rho_s)_{ij} = m^2(\Upsilon_s)_{ij} = (n_0 m\delta_{ij} + a_E m^2 q_i q_j)$. Thus we have shown that the system under study is superfluid and the helicity modulus and the superfluid mass density are anisotropic tensor quantities.

One can come to similar conclusions starting from definitions (4). The noncondensate contribution to the total current is then given by

$$\frac{\mathfrak{J}'}{S} = \frac{\hbar}{2mi\,S}\int \langle \hat{\Psi}'^{+}(\mathbf{r})\nabla\hat{\Psi}'(\mathbf{r}) - [\nabla\hat{\Psi}'^{+}(\mathbf{r})]\hat{\Psi}'(\mathbf{r})\rangle d\mathbf{r}$$
$$= \frac{\mathbf{P}}{m}n' + \frac{1}{m(2\pi)^2}\int d\mathbf{p}\mathbf{p}\{|v_{\mathbf{p}}^0|^2 + V_0^2|v_{\mathbf{p}}^+|^2$$
$$+ V_0^2|v_{\mathbf{p}}^-|^2 + 2V_0^2 v_{\mathbf{p}}^0\Delta v_{\mathbf{p}}^0\} + \hbar\mathbf{q}V_0^2\{|v_{\mathbf{p}}^+|^2 - |v_{\mathbf{p}}^-|^2\}.$$

From the calculations above we can quantitatively discuss anisotropy of sound velocity. It can be obtained from the spectrum (17) as $C_s = \partial\varepsilon_{\mathbf{p}}/\partial p|_{p,P=0}$ yielding

$$C_s = \sqrt{\frac{n_0 U_0}{m}}\left(1 - \frac{V_0^2}{(T+2U)^2}\cos^2\varphi + \frac{V_0^2(T-U)U_{\mathbf{q}}}{U_0(T+2U)^3}\right), \tag{22}$$

where φ is the angle between $\mathbf{p}$ and $\mathbf{q}$. One can see the presence of an anisotropic contribution in (22). It is interesting to note that corrections to (17) due to periodic potential become unimportant as $p \to \infty$. One can prove that $\Delta\varepsilon_{\mathbf{p}} \to$ constant if $|\mathbf{p}| \to \infty$, becoming negligible compared to $\varepsilon_0(\mathbf{p})$.

To demonstrate the physics of anisotropic superfluidity we would also like to calculate Υ_s. The calculation can be carried out properly with the help of the relation [91]

$$C_s(\phi) = \sqrt{\frac{d\mu}{dn}\Upsilon_s(\phi)},$$
$$\frac{d\mu}{dn} = \frac{d\mu}{dn_0}\left(\frac{dn}{dn_0}\right)^{-1}, \tag{23}$$

where ϕ is the angle between $\mathbf{q}$ and $\mathbf{v}$ and all the quantities are taken at $\mathbf{P} = 0$.

The condensate depletion is $n' \approx n_0 m U_0/(2\pi\hbar^2)$; i.e., we have $n_0(dn/dn_0) = n$. One obtains using (22)

$$\Upsilon_s(\phi) = \frac{n}{m}\left(1 - 2\frac{V_0^2}{(T+2U)^2}\cos^2\phi\right). \tag{24}$$

As is discussed in Sec. II [see Eqs. (2), (4)], the helicity modulus is in general case a tensor. To illustrate this we rewrite Eq. (24) in tensor form [114]:

$$||\Upsilon_s|| = \frac{n}{m}\begin{pmatrix} 1-2\Delta_s & 0 \\ 0 & 1 \end{pmatrix}, \tag{25}$$

where the x axis is along the wave vector and the anisotropy parameter Δ_s is defined as follows:

$$\Delta_s = \frac{V_0^2}{(T+2U)^2}. \tag{26}$$

It is useful to consider a particular case where the form of $\Upsilon_s(\phi)$ is known. Let us consider a case when $|\mathbf{q}| \to \infty$, $U_{\mathbf{p}} = U_0 =$ constant. In this case it should be possible to explain the anisotropy of Υ_s from an effective mass point of view. The effect of an external potential $V(\mathbf{r})$ is then reduced to substitution of the initial mass with a tensor m_{ij} determined from a single-particle problem in the potential $V(\mathbf{r})$. With accuracy up to the second order in V_0 in coordinates where the x axis is along $\mathbf{q}$, m_{ij} has the form

$$m_{ij} = m_i\delta_{ij},\ m_1 = m + 8m^3V_0^2/(\hbar\mathbf{q})^4,\ m_2 = m.$$

Energy calculation for motion with probe momentum $\mathbf{P}$ leads us to

$$\left.\frac{E}{S}\right|_{\mathbf{P}\to 0} \approx \frac{E(\mathbf{P}=0)}{S} + \frac{1}{2}\sum_{ij}(m)_{ij}^{-1}P_iP_j.$$

Then we have from the definition (3)

$$\Upsilon_s(\phi) = \frac{n}{m + 8m^3V_0^2/(\hbar\mathbf{q})^4}\cos^2\phi + \frac{n_s}{m}\sin^2\phi$$
$$\approx \frac{n}{m}\left[1 - 8m^2V_0^2/(\hbar\mathbf{q})^4\cos^2\phi\right],$$

which coincides with (24).

Thereby we have shown the presence of a BEC, superfluidity and a diagonal long-range order in the system and demonstrated anisotropy of superfluid properties. However, despite the occurrence of BEC, superfluidity, and diagonal long-range order, the system it is not a real supersolid. Indeed, the diagonal long-range order does not involve the possibility of static deformations because the order is created artificially by the external potential. In a true supersolid, on the contrary, the modulations emerge due to self-organization, caused by the instability of the homogeneous phase with respect to the formation of periodic (crystalline) modulation in the density profile, static deformations being possible.

The results obtained can be generalized for spatial lattices additively for energy, spectrum, and condensate depletion because all of the equations studied were linearized and for energy and current cross terms stemming from different modulation wave vectors vanish after integration. For a limit $|\mathbf{q}| \to \infty$, $U_{\mathbf{p}} = U_0 =$ constant and a square or triangular lattice one can see that anisotropy of helicity modulus and superfluid mass density is absent. It is also convenient to generalize results for three-dimensional systems; the only peculiarity is an additional constraint $2U_{\mathbf{p}} - U_{\mathbf{p}+\mathbf{q}} - U_{\mathbf{p}-\mathbf{q}} = O(\frac{1}{|\mathbf{p}|^{1+\beta}})$, $\beta > 0$, $|\mathbf{p}| \to \infty$ for the noncondensate energy to converge.

A straightforward generalization can be also obtained in the case when there is an intrinsic mass anisotropy. An answer for the helicity modulus can be obtained for this case by transforming the tensor (25) to the frame where the mass tensor is diagonal and changing the definition of Δ_s:

$$||\Upsilon_s|| = \begin{pmatrix} n_0/m_1 - A_1 & -A_{12} \\ -A_{12} & n_0/m_2 - A_2 \end{pmatrix}, \tag{27}$$

where

$$A_1 = 2\frac{V_0^2\hbar^2q_1^2n_0}{T'(T'+2U)m_1^2},\quad A_2 = \frac{V_0^2\hbar^2q_2^2n_0}{T'(T'+2U)m_2^2},$$
$$A_{12} = \frac{V_0^2\hbar^2q_1q_2n_0}{T'(T'+2U)m_1m_2},\quad T' = \frac{\hbar^2q_1^2}{2m_1} + \frac{\hbar^2q_2^2}{2m_2},$$

with q_1 and q_2 being the components of $\mathbf{q}$ in the principal axes frame of the mass tensor and m_1, m_2 are its eigenvalues.

IV. PHYSICAL REALIZATION

To observe the effects described in Sec. III we propose to use a system of dipolar excitons in a QW (or coupled QWs) in an external electrostatic field created by electrodes sputtered on the sample. A principal scheme of the realization discussed is shown in Fig. 3. The bottom electrode is a flat layer of a doped semiconductor. The top one consists of periodically arranged (with period $a + b$) metallic stripes of width a, with the separation between them being b. We assume the thickness of the stripes to be small enough for the top electrode to be semitransparent for recombination radiation of photons.

The inhomogeneous electrostatic field appearing when voltage is applied to the electrodes creates a periodic potential for the excitons in the QW plane by interacting with their dipole moment. The period λ of the potential depends on the overall period of the top electrode $a + b$ as well as on the

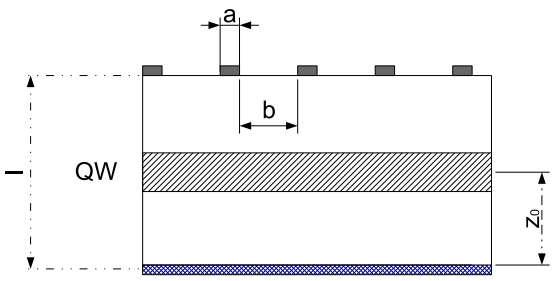

FIG. 3. Cross-sectional sample scheme. Dark areas on the top are the metallic stripes of the upper electrode, shaded area in the middle is the QW region, and shaded area at the bottom is the lower electrode.

distribution of voltages on them (for the case in which it is not uniform). Magnitude of the applied voltage determines the amplitude of potential oscillations V_0 as well as the constant component $\mathbf{E}_{\rm av} = \{0,0,E_z^{\rm av}\}$ of the electric field. The latter determines the dipole moment of the excitons in single QWs and their lifetime in the radiation zone [115].

The proposed realization has two important limitations. First, for observing excitons in a superfluid state it is necessary for them to be in thermodynamic equilibrium. This happens only if the excitons' relaxation time is not larger than their lifetime determined by recombination processes. The second limitation arises because of the presence of an electric field component parallel to the QW plane in electrostatic traps. In the case when dipole energy becomes on the order of the exciton binding energy, the electron and hole may tunnel to an unbound state which leads to large leakage and prohibits observation of condensation [116].

Now we discuss experimental manifestations of anisotropic superfluidity in the proposed realization following the results of Sec. III. First of all we note that the density of the condensate is periodically modulated [see (8), (9)]. In the case of direct optical recombination of excitons this will lead to additional features in their luminescence. For a uniform condensate luminescence is normal to the QW plane [29] with wave vector k_z given by $E_g/\hbar c$, where E_g is the excitonic gap and c is the speed of light in vacuum. In the presence of a modulation $\Phi(\mathbf{r})$ contains harmonics carrying momentum $\pm\mathbf{q}$. This momentum can be transferred to photons leading to the appearance of two additional luminescence rays with momentum $(\pm\mathbf{q},\sqrt{k_z^2-q^2})$. They will be directed at angles $\theta_{lum} = \pm\arcsin(|\hbar\mathbf{q}|c/E_g)$ with respect to the normal to the QW plane in the cross-sectional plane (see Fig. 4). The intensity of these additional rays will be proportional to $|\Phi_\pm|^2$ [see Eq. (8)]. In the case of an external potential consisting of more than one harmonic, the above considerations lead to a "fan" (in the 1D case) or a "lattice" of additional luminescence rays (a similar effect has been predicted for stimulated many-photon recombination of an exciton BEC in [50]). Note that in our model the order parameter should contain higher harmonics; however, their intensity is small. The magnitude of the second harmonic should be $\sim O([V_0/(T+2U)]^2)$ and thus the intensity of corresponding luminescence rays is on the order of $\sim O([V_0/(T+2U)]^4)$ compared to the central ray.

As a direct consequence of the superfluid density anisotropy, the shape of the angle-resolved luminescence

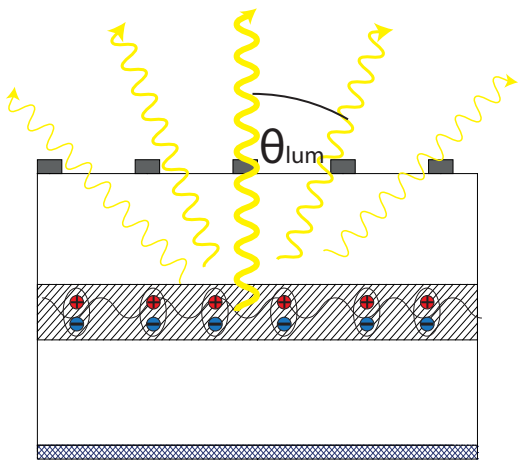

FIG. 4. Luminescence of a modulated excitonic condensate. Additional rays appear due to the oscillations of the order parameter, with the higher harmonics being suppressed. Thickness of the wavy lines corresponds to the intensity of the radiation. The upper electrode is semitransparent and its effect on the luminescence can be neglected.

profile close to the normal direction is elongated along $\mathbf{q}$ and compressed in the perpendicular direction. At finite temperatures the intensity of the quasicondensate luminescence can be calculated by means of the hydrodynamic method in quantum field theory [91,117–119] with the result being [120]

$$I(\vartheta,\varphi) = K\frac{(\tilde{c}E_g/cT)^\gamma}{[\sin^2\vartheta(1-2\Delta_s\cos^2\varphi)]^{1-\gamma/2}},$$
$$K = \frac{K_0E_gmT\eta}{(2\pi\hbar)^2\tau_{\rm bright}},\quad \gamma = \frac{mT}{2\pi\hbar^2n\sqrt{1-2\Delta_s}}, \tag{28}$$

where ϑ is the angle between the luminescent ray and the normal to the QW plane, $\tilde{c} = \sqrt{U_0n/m}$, $K_0 \sim 1$ is a dimensionless constant, $\tau_{\rm bright}$ is the exciton lifetime in the radiative zone, $\eta = N_0/N$ is the zero-temperature condensate fraction, and T is the exciton temperature, which is assumed to be finite, but low enough [121]. Rays corresponding to higher harmonics of the anisotropic potential acquire analogous anisotropic shape.

Moreover, the luminescence spectrum also acquires an anisotropic form:

$$I(\vartheta,\varphi,\omega) = I^0_{\varphi\vartheta}\delta(E_g+\mu-\varepsilon_{\varphi\vartheta}-\hbar\omega),$$
$$I^0_{\varphi\vartheta} = \frac{K_0E_g^3}{(2\pi\hbar c)^2\tau_{\rm bright}}\int|v_{\mathbf{o}}|^2\frac{d\mathbf{r}}{S}, \tag{29}$$
$$\varepsilon_{\varphi\vartheta} = \left(C_s^{\pi/2}/c\right)E_g\sin\vartheta\sqrt{1-2\Delta_s\cos^2\varphi},$$

where $o_x = q_r\sin\vartheta\cos\varphi$, $o_y = q_r\sin\vartheta\sin\varphi$, $q_r = E_g/\hbar c$, the dependence of $v_{\mathbf{o}}$ on $\mathbf{r}$ is given by (14), and $C_s^{\pi/2}$ is equal to C_s [see (22)] for $\varphi = \pi/2$. It is remarkable that the luminescence frequency in (29) depends on the in-plane angle φ. The frequency shift between the directions $\varphi = 0$ and $\varphi = \pi/2$ is then given by

$$\delta\omega = \left(C_s^{\pi/2}/c\right)E_g\sin\vartheta(1-\sqrt{1-2\Delta_s}), \tag{30}$$

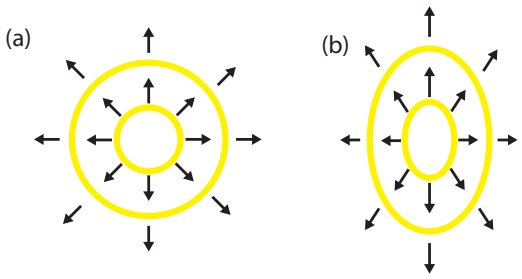

FIG. 5. Qualitative depiction of the propagation of a (a) circular and (b) elliptic wave from a point source through isotropic and anisotropic superfluid exciton BEC, correspondingly. Length of the arrows corresponds to the magnitude of the sound velocity in the corresponding direction. The smaller axes of the ellipses are directed along $\mathbf{q}$.

which is evidently nonzero and is determined by the anisotropy parameter Δ_s. A similar effect takes place for the rays corresponding to higher harmonics of the order parameter as well as for the luminescence along the normal to the QW plane if an in-plane magnetic field is applied [122–124].

Anisotropy of the excitation spectrum (17) is at the heart of a number of observable phenomena. First of all, one can directly measure the spectrum experimentally. Techniques for such measurements are known for systems of excitons [122] and have been described in the literature. Anisotropy of sound velocity (22) can be investigated by a direct measurement as well [122]. A different option also exists: as a consequence of the anisotropy of sound, circular waves should become *elliptic* with the ratio between axes equal to C_s^x/C_s^y (Fig. 5). An elliptical wave can be created by an abrupt change of local chemical potential [125] caused by a voltage applied to a region of the upper electrode [73,75]. The propagation of the wave can be observed then in a time-resolved luminescence experiment [126].

Another quantity we are interested in is the helicity modulus (24). To determine $\Upsilon_s(\phi)$ we propose to create 2D excitons by spatially resolved continuous wave pumping, with an in-plane magnetic field being applied in the QW plane during the pump. As is known [123], the presence of crossed out-of-plane electric and in-plane magnetic fields results in a shift of exciton spectrum in the momentum space. The dispersion law takes then the form

$$\varepsilon_0(\mathbf{p}_B) = \frac{(\mathbf{p}_B - \mathbf{p}_0)^2}{2m}, \quad \mathbf{p}_0 \equiv \mathbf{B}_\parallel \times \mathbf{d}_0/c. \tag{31}$$

Here $\mathbf{p}_B$ is the magnetic momentum, $\mathbf{p}_0$ is the shift momentum, $\mathbf{B}_\parallel$ is the in-plane magnetic field, and $\mathbf{d}_0$ is the exciton dipole moment. We also neglect the change in the exciton effective mass due to the magnetic field because we assume $\mathbf{B}_\parallel$ to be small and the correction is quadratic in $\mathbf{B}_\parallel$.

After the collisional relaxation (local thermalization inside the exciton gas) [15,127] and the phonon relaxation (cooling of the locally equilibrated exciton gas) [128] exciton occupancy $n(\mathbf{p}_B)$ "falls" down to the bottom of the shifted parabola ($\mathbf{p}_B \approx \mathbf{p}_0$). In this state the exciton system is "cold" and the group velocity of excitons averaged over $n(\mathbf{p}_B)$ is zero [129]:

$$\mathbf{v}_0 \equiv \langle \partial\varepsilon_0(\mathbf{p}_B)/\partial\mathbf{p}_B \rangle = \langle \mathbf{p}_B - \mathbf{p}_0 \rangle/m = 0. \tag{32}$$

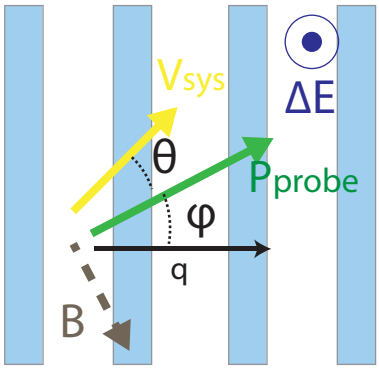

FIG. 6. Noncollinearity of the nondissipative flow and the probe momentum in an anisotropic superfluid. ϕ is the angle between P_{probe} and the periodic potential orientation; θ is the angle between the direction of the nondissipative flow and the probe momentum. The in-plane magnetic field $\mathbf{B}$ (gray) is oriented perpendicularly to the probe momentum, while the variation of the polarizing electric field $\delta\mathbf{E}$ (dark blue) is oriented perpendicularly to the QW plane.

The system is then at rest despite the dispersion law shift. The cooled excitons flowing to the examined area after their global thermalization and transition into the superfluid state will thus also have a shifted magnetic momentum $\langle \mathbf{p}_B \rangle = \mathbf{p}_0$.

Suppose now that $\mathbf{p}_0$ changes with time $\mathbf{p}_0 \to \mathbf{p}_0 - \mathbf{P}$, where $\mathbf{P}$ depends on time adiabatically slow. The normal component will remain at rest due to relaxation processes [130], while the superfluid component will be set into motion. The resulting system velocity will be related to the probe momentum $\mathbf{P}$ through the helicity modulus tensor [see Eq. (4)]. Thus the helicity modulus can be measured.

One way to implement the idea above is to change slowly the polarizing electric field $E_z^{\text{av}} \to E_z^{\text{av}} + \Delta E_z^{\text{av}}(t/\tau_{\text{sw}})$, where τ_{sw} is the characteristic switching time. This results in a change of the exciton dipole moment $\mathbf{d}_0 \to \mathbf{d}'(t/\tau_{\text{sw}}) \equiv \mathbf{d}_0 + \Delta\mathbf{d}(t/\tau_{\text{sw}})$ and thus changes the bottom of the shifted parabola [see (31)], i.e., the quantity $\mathbf{P}$.

Let us discuss the limitations on the electric field switching time. It is bound from above by the exciton lifetime because in a stationary regime the excitons created by the pump will replace the recombined ones leading to a large number of excitons having momentum lower then the probe one in the system. In contemporary exciton luminescence experiments electric field switching occurs on time scales down to 100 picoseconds [131] which is guaranteed to be smaller than the usual exciton lifetimes. The lower boundary follows from the fact that in the course of a nonadiabatic perturbation transitions to excited states may occur destroying superfluidity and even heating the system.

As has been discussed in Sec. II, the total current in the system is related to the probe momentum through the helicity modulus tensor and can be noncollinear to it (Fig. 6). To determine the total current one must know the total density and the velocity of the system's motion. Both quantities can be measured from the recombination luminescence of excitons: the intensity is proportional to the total density and the direction and the magnitude of the velocity can be determined by observing movement of the radiating excitonic spot. Thus knowing the probe momentum from field parameters it is

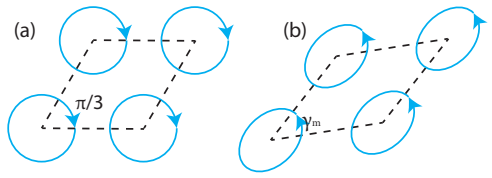

FIG. 7. Unit cell of the vortex lattice (a) without or (b) with an external periodic potential. We assume that the periodic potential wave vector is oriented along the small diagonal of the unit cell.

possible to determine the helicity modulus. Note that in sufficiently high magnetic fields exciton recombination is suppressed [122]; however, phonon-assisted luminescence [132] should make the observation of exciton motion nevertheless possible.

There is also a method to measure anisotropy of helicity modulus indirectly. "Stirring" a condensate with a frequency greater then a critical one is known to lead to formation of quantized Feynman vortices in the system [133]. Such a "stirring" can be performed for indirect dipolar excitons by a radial in-plane magnetic field [48]. In an isotropic case the vortices are expected to form a triangular lattice [see Fig. 7(a)] as a consequence of radially symmetric intervortex interactions. In a weak anisotropic case, however, the symmetry of equilateral triangle type is lost [see Fig. 7(b)]. The unit cell is deformed due to an effective rescaling of coordinates [96,102] $x \to x/\eta$, $y \to \eta y$, $\eta = [(\mathrm{Y}_s)_{xx}/(\mathrm{Y}_s)_{yy}]^{1/4}$. Thus the difference between the minimal angle γ_m of the unit cell and $\pi/3$ allows one to measure the anisotropy of the helicity modulus.

V. ESTIMATION OF THE OBSERVABLE EFFECTS

Now we will consider four particular setups, based on the existing structures for exciton condensation observations. Parameters of these structures are given in the upper section of Table I. In the two of these setups (GaAs/AlGaAs and MoS_2/hBN coupled QWs) applied voltage is uniform and thus $\lambda = a + b$.

We have estimated the magnitude of the predicted effects for experimental setups described in Table I. First of all one needs to estimate parameters of the model (5). The interaction between indirect excitons cannot be taken simply as $U_0(r) = (2e^2/\varepsilon)(1/r - 1/\sqrt{r^2 + D^2})$, because in the dipolar limit $D \to 0$, $eD =$ constant the Fourier transform of this potential is singular. One has thus to take into account the renormalizations stemming from ladder diagrams and related to the scattering problem [111]. We use instead a model potential $U(\mathbf{p})$, which is defined as follows. Its "contact" part $U_0 = U(0)$ is deduced from the results of a quantum Monte Carlo simulation for a system of dipoles without periodic modulation [124]. The "long-range" part of the potential $U(\mathbf{p}) - U_0$ is then taken to be the same as for $U_0(r)$ (this quantity does not diverge even in the dipolar limit). Details of the estimates are given in Appendix A 1. Actually, the form of the potential (A3), (A4) leads to interesting qualitative results regarding the anisotropy parameter Δ_s. In Fig. 8, for the GaAs/AlGaAs/GaAs CQW structure q is small such that $\Delta_s \approx [V_0/(2U_0 n_0)]^2$. Consequently, as D increases, the dipole-dipole interactions become stronger and Δ_s is strongly

TABLE I. Upper section: Material parameters for the coupled GaAs/AlGaAs QWs [70], single GaAs/AlGaAs QW [10,134], coupled MoS_2/hBN QWs [60], and coupled $MoSe_2$/hBN/WSe_2 QWs [62,63]. Given are the values for the excitonic gap E_g, the QW width L_{QW} and the barrier width L_B, and the distances between QW(s) and the bottom electrode z_0 and between the top and the bottom electrodes l. Lower section: Excitonic parameters for the model (5). Given are the values for the exciton density n, $n \approx n_0$, the chemical potential μ, the amplitude of the external periodic potential V_0, the characteristic kinetic energy contribution $\hbar^2 q^2/2m$, and the estimate for $T_c \approx \pi\hbar^2 n_s/2m$ for the superfluid transition temperature, where we set [136] $n_s = n_0\sqrt{1-2\Delta_s}$.

Quantity	GaAs/ AlGaAs/ GaAs CQWs	GaAs/ AlGaAs SQW	MoS_2/ hBN/ MoS_2 CQWs	$MoSe_2$/ hBN/ WSe2 CQWs
E_g (eV)	1.55	1.51	1.8	1.3
L_{QW} (nm)	8	40	0.333	0.333
L_B (nm)	4		1.667	1
l (nm)	1000	120	11	11
z_0 (nm)	100	60	8	8
a (nm)	500	60	6	6
b (nm)	500	70	7	6
λ (nm)	1000	130	13	12
n_0 (10^{10} cm^{-2})	0.8	1	80	160
μ (meV)	0.5	1.1	16.9	27.0
$\hbar^2 q^2/2m$ (meV)	6.8×10^{-3}	0.40	8.9	11.9
V_0 (meV)	0.15	0.40	8.1	7.8
T_c (K)	0.5	0.48	6.8	23.8

suppressed. For the MoS_2/hBN/MoS_2 CQW structure, on the contrary, an increase or a very slow decrease of Δ_s can be observed. The explanation is that for this case the position of a rotonic-like minimum of the function $k^2/2m + 2U(\mathbf{k})n_0$ is very close to $\mathbf{q}$. In strongly correlated systems the position of the rotonic minimum is given by $2\pi\hbar\sqrt{n}$ [124,135] which nearly coincides with $q = 2\pi\hbar/\lambda$ for density 0.6×10^{12} cm^{-2}

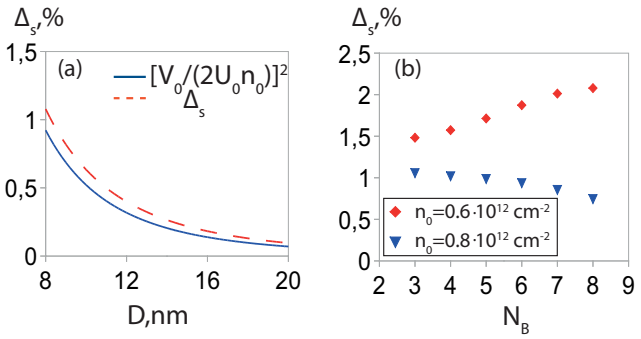

FIG. 8. Dependence of Δ_s on the e-h separation distance. (a) GaAs/AlGaAs/GaAs CQW structure with $V_0 = 0.05$ meV. Δ_s approximately follows $[V_0/(2U_0 n_0)]^2$. (b) MoS_2/hBN/MoS_2 CQW structure, $V_0 = 1.4$ meV, for two values of exciton densities 0.6×10^{12} cm^{-2} (orange diamonds) and 0.8×10^{12} cm^{-2} (blue triangles). Number of hBN barrier monolayers N_B is used instead of D. For parameters not given here see Table I.

($\lambda = 13$ nm from Table I, $1/\sqrt{n} = 12.9$ nm). Thus, for this case $T + 2U$ is expected to decrease when interactions become stronger, until an instability is reached [41]. Here we restrict our considerations to systems without rotonic instability and we have checked that for the parameters used in Table I the excitation spectrum (17) is stable.

Let us move to calculations for realistic system parameters. Calculation of the electric field configuration in the QW plane (including estimates for E_z^{av} and V_0) is presented in Appendix A 2. Single-exciton properties, such as the electron-hole separation, the lifetime, and the binding energy, have been obtained from a numerical solution of the Schrödinger equation. This is discussed in detail in Appendix A 3.

We turn now to the helicity modulus measurement procedure described in Sec. IV. If the direction of the probe momentum constitutes an angle ϕ with the x axis the angle θ between the system's velocity $\mathbf{v}_{\mathrm{sys}}$ and probe momentum (see Fig. 6) is

$$\theta = \arccos \frac{1 - 2\Delta_s \cos^2\phi}{\sqrt{1 - 4\Delta_s \cos^2\phi + 4\Delta_s^2 \cos^2\phi}}, \tag{33}$$

where Δ_s is the anisotropy parameter defined in (26). This angle is maximal at a certain $\phi = \phi_m$ and has value θ_m:

$$\phi_m = \arccos \frac{1}{\sqrt{2(1-\Delta_s)}}, \quad \theta_m = \arccos \frac{\sqrt{1-2\Delta_s}}{1-\Delta_s}. \tag{34}$$

Moreover, we have estimated the velocity acquired by the system after the electric field switching procedure discussed in Sec. IV. For GaAs structures it is 3.2×10^5 cm/sec for coupled QWs and 9.6×10^5 for a single QW in magnetic field $B_{\parallel} = 8$ T (see details in Appendix A 4). However, for the other two structures this method has turned out to be unfeasible. Alternative ways are to create a gradient of a local chemical potential of excitons [78] or to move a macroscopically coherent exciton system along a narrow channel [137].

Now we move onto the indirect effects discussed in Sec. IV. Their magnitude can also be related to Δ_s. Ratio of the axes of an elliptical wave is $C_s^x/C_s^y \approx 1 - \Delta_s$. Thus a good measure of anisotropy is the quantity $\delta C_s/C_s = 1 - C_s^x/C_s^y$. Calculation of the minimal angle in the deformed vortex lattice unit cell is also straightforward for the case when the period of the vortex lattice is much larger than λ, as one can simply rescale the parameters of the unit cell. We assume that the principal axes of the helicity modulus tensor are along the diagonals of the unit cell (which is a rhombus). If the x axis is along the larger diagonal then it is contracted by a factor of $\sqrt{1-2\Delta_s}$. It follows then that the minimal angle in the unit cell γ_m is

$$\gamma_m = \arccos \frac{1+\Delta_s}{2-\Delta_s}. \tag{35}$$

A measure of the anisotropy of quasicondensate luminescence intensity for directions close to normal to the QW plane is given by

$$\delta I/I = [I(\vartheta,0) - I(\vartheta,\pi/2)]/I(\vartheta,0) = 2\Delta_s. \tag{36}$$

The corresponding frequency shift between the luminescence along and across $\mathbf{q}$ is given by (30).

All of the results of estimations discussed above are summarized in Table II. One can see that the anisotropy effects are weak for large λ. However if λ becomes on the order of the interexciton distance, the effects are considerably enhanced, so that an intermediate anisotropy regime $(\Upsilon_s)_{yy}/(\Upsilon_s)_{xx} \sim 3$ is realized.

TABLE II. Estimates for the predicted effects for structures described in Table I. Given are the values for the anisotropy parameter Δ_s, the angle of motion of superfluid component ϕ_m and the anisotropy angle for the superfluid flow θ_m (34), the anisotropy of the sound velocity $\delta C_s/C_s$, the lowest angle in the triangular unit cell of vortex lattice γ_m (35), the ratio of the diagonal components of the helicity modulus tensor $(\Upsilon_s)_{yy}/(\Upsilon_s)_{xx}$, and the degree of the quasicondensate luminescence intensity anisotropy $\delta I/I$ (36) as well as frequency anisotropy $\delta\omega = \omega(\vartheta,0) - \omega(\vartheta,\pi/2)$ for $\vartheta = 5\pi/12$ [see (30)].

Quantity	GaAs/ AlGaAs/ GaAs CQWs	GaAs/ AlGaAs SQW	MoS_2/ hBN/ MoS_2 CQWs	$MoSe_2$/ hBN/ WSe2 CQWs
Δ_s	2.9%	21.4%	31.1%	5.5%
ϕ_m	44°	37°	32°	43°
θ_m	1.7°	15.8°	26.9°	3.3°
v_{sys}/v	0.97	0.76	0.61	0.94
$\delta C_s/C_s$	3%	24%	39%	6%
γ_m	58.6°	47.1°	39.1°	57.2°
$(\Upsilon_s)_{yy}/(\Upsilon_s)_{xx}$	1.06	1.8	2.6	1.1
$\delta I/I$	5.7%	42.9%	62.2%	10.9%
$\delta\omega$, μeV	2.9	35.8	126.9	17.4

In Sec. IV we have also discussed the limitations which our system should satisfy. In Appendix B a detailed discussion of these limitations is presented with the conclusions that setups considered here do satisfy the necessary conditions.

VI. CONCLUSION

In the article, we have demonstrated anisotropy of the helicity modulus, sound velocity and angle-resolved luminescence spectrum for a moving two-dimensional gas of weakly interacting bosons in a one-dimensional external periodic potential. Analytical expressions for anisotropic corrections to the excitation spectrum (17), sound velocity (22), and helicity modulus (24), (25) have been obtained with the Bogoliubov technique at $T = 0$. An expression for angle-resolved photoluminescence intensity (28) has been obtained at low temperatures by means of quantum-field hydrodynamics. The considered model can be used to describe a physical system of dipolar excitons in a QW in an electrostatic lattice. Our calculations can be also applied to systems of dipolar atoms in optical lattices in periodic fields. Our results can be straightforwardly generalized for more complicated forms of periodic potentials as well as systems with intrinsic anisotropy of mass (27). We have not taken exciton spin into account, as in the considered regime (see Sec. III) these can be neglected.

We propose several qualitative manifestations of excitonic anisotropic superfluidity:

(1) The photoluminescence of the excitonic system is organized into a pattern of discrete rays with intensity decreasing away from the normal to the QW plane (see Fig. 4). At finite

temperatures, due to luminescence of a 2D quasicondensate of excitons each ray has a finite angular extent and an elliptic, rather then circular, shape. This effect is directly related to the anisotropy of the helicity modulus [see Eq. (28)].

(2) The unit cell of the triangular vortex lattice, appearing in a radial magnetic field [48] in the QW plane, will not be equilateral.

(3) Collisionless sound waves created by a pointlike source will be elliptical instead of circular.

(4) The momentum transferred to the system will not be collinear to the resulting nondissipative current.

(5) The frequency of the angle-resolved luminescence arising from the noncondensate excitons depends on the in-plane direction of the beam (i.e., polar angle φ). Moreover, if an in-plane magnetic field is applied, the luminescence frequency along the normal to the QW plane depends on the direction of the field.

We have also proposed an experiment to determine the helicity modulus tensor including a method for setting dipolar particles into motion which is valid for other realizations such as atomic systems. Using the results of simulations [124] estimates for the magnitude of the predicted effects and manifestations of anisotropic superfluidity have been given. For one of the considered structures we have observed an increase in anisotropy due to closeness of the position of a rotonic-minimum-like feature in the interexciton potential $U(\mathbf{p})$ to $\mathbf{q}$ (Fig. 8). The magnitudes of anisotropic effects in Table II give evidence for possibility of their observation and detection in GaAs/AlGaAs heterostructures as well as MoS_2/hBN/MoS_2 and $MoSe_2$/hBN/WSe_2 bilayers in future experiments.

ACKNOWLEDGMENT

The work was supported by grant Russ. Sci. Found. 17-12-01393.

APPENDIX A: DETAILS OF CALCULATIONS

1. Calculation of the exciton-exciton interaction potential

Neglecting fermionic and spin effects for the excitons, one can write the Fourier transform $U_{\mathbf{p}}$ of the pseudopotential $U(\mathbf{r})$ of the exciton-exciton interaction as

$$U_{\mathbf{p}} = U_0 + \int d\mathbf{r}\left(e^{-\frac{i}{\hbar}\mathbf{pr}} - 1\right)U(\mathbf{r}), \tag{A1}$$

where $U_0 = U_{\mathbf{p}}|_{\mathbf{p}=0}$. In the second term in (A1) we substitute $U(\mathbf{r})$ with the bare interexciton interaction in an e-h bilayer:

$$U_0(\mathbf{r}) = \frac{2e^2}{\varepsilon}\left(\frac{1}{r} - \frac{1}{\sqrt{r^2 + D^2}}\right). \tag{A2}$$

As a result (A1) takes the form

$$U_{\mathbf{p}} = U_0 + \frac{4\pi d^2}{\varepsilon D}\left(\frac{1 - e^{-pD/\hbar}}{pD/\hbar} - 1\right), \tag{A3}$$

where $d = eD$.

We cannot, however, simply use $U_0 = \int U_0(\mathbf{r})d\mathbf{r}$ to calculate U_0 in (A3), because this function shows a diverging behavior for dipolar interactions [$U_0(r) = d^2/r^3$ has an unintegrable singularity at $\mathbf{r} = 0$]. Instead we use the results of an *ab initio* modeling [124] performed for dipolar excitons:

$$U_0 = \frac{\hbar^2}{m}\frac{\partial^2}{\partial \bar{n}^2}\bar{n}e_0(\bar{n}). \tag{A4}$$

Here $\bar{n} = nm^2d^4/(\hbar^4\varepsilon^2)$, dimensionless density, and

$$e_0(\bar{n}) = a_e \exp(b_e \ln\bar{n} + c_e \ln^2\bar{n} + d_e \ln^3\bar{n} + e_e \ln^4\bar{n}), \tag{A5}$$

dimensionless ground-state energy per particle, where coefficients $a_e = 9.218$, $b_e = 1.35999$, $c_e = 0.011225$, $d_e = -0.00036$, and $e_e = -0.0000281$, correspond to an interval $1/256 \leqslant \bar{n} \leqslant 8$. For all numerical estimates we replace n by n_0 in (A4) and (A5) due to the condition $(N - N_0)/N \ll 1$ (see Sec. III).

2. Electric field distribution in QW plane

Electrostatic field configuration in the QW plane can be calculated analytically: neglecting inhomogeneities in the charge distribution over the stripes of the upper electrode the problem is solved by the image method with respect to the bottom electrode plane (see setup in Fig. 3). Assuming the thickness of stripes to be small and denoting charge of a stripe per unit area as σ we have

$$\begin{aligned}
E_x(x,z) &= \frac{\sigma}{\varepsilon}\sum_{j\in Z}\left[\ln\left(\frac{[(x - a - j\lambda)/l]^2 + [1 + z/l]^2}{[(x - j\lambda)/l]^2 + [1 + z/l]^2}\right) - \ln\left(\frac{[(x - a - j\lambda)/l]^2 + [1 - z/l]^2}{[(x - j\lambda)/l]^2 + [1 - z/l]^2}\right)\right],\\
E_y(x,z) &= 0,\\
E_z(x,z) &= \frac{2\sigma}{\varepsilon}\sum_{j\in Z}\left[\arctan\left(\frac{a/l}{[1 - z/l][(x - j\lambda - a)(x - j\lambda)/(l - z)^2 + 1]}\right)\right.\\
&\quad\left. + \arctan\left(\frac{a/l}{[1 + z/l][(x - j\lambda - a)(x - j\lambda)/(l + z)^2 + 1]}\right)\right],
\end{aligned} \tag{A6}$$

where ε is the dielectric constant and $\sigma = \varepsilon E_z^{\mathrm{av}}\lambda/4\pi a$.

We calculated the field configurations for four setups (see Table I) with E_z^{av} given in Table III. Summation in (A6) was carried out numerically with relative error estimate 10^{-13}. The result for the first structure is presented in Fig. 9. One can see that the oscillations of the electric field have a well-defined period equal to $a + b$. This means that if we decompose $E_z(x,z_0) = E_z^{(0)} + \Delta E_z\cos[2\pi(x - x_0)/\lambda] + E_z^{(2)}\cos[4\pi(x - x_0)/\lambda] + \cdots$ then $E_z^{(n)} \ll \Delta E_z$. We verified

TABLE III. Electrostatic field parameters in the QW plane for the structures in Table I. $E_z^{\rm av}$ is the constant component of the field; ΔE_z and ΔE_x are the amplitudes of first harmonic along z and x.

Quantity	GaAs/ AlGaAs/ GaAs CQWs	GaAs/ AlGaAs SQW	MoS_2/ hBN/ MoS_2 CQWs	$MoSe_2$/ hBN/ WSe2 CQWs
$E_z^{\rm av}$ (kV/cm)	40	5.8	256	447
ΔE_z (kV/cm)	0.11	0.22	40	58
ΔE_x (kV/cm)	0.06	0.22	41.8	60.0

this by numerical convolution with higher harmonics. For all structures we found that the component along z has a constant component $E_z^{\rm av}$ and an oscillating component with amplitude ΔE_z, while the field along x is purely oscillatory with amplitude ΔE_x (numerical values presented in Table III).

The role of the constant component $E_z^{\rm av}$ is to fix the dipole moment of the excitons while ΔE_z determines V_0 in the model (5). Component $E_x(x,z)$ is oriented in the QW plane and can cause, as has been discussed above, dissociation of the excitons. However, if the energy associated with this field is less then the binding energy of an exciton, dissociation is forbidden. For corresponding estimates see Appendix B.

3. Calculation of the electron-hole separation, the exciton lifetime, binding energy, and radius

Electron-hole separation is given by

$$D = \left| \int \left(\psi_h^2(z) - \psi_e^2(z)\right) z dz \right|,$$

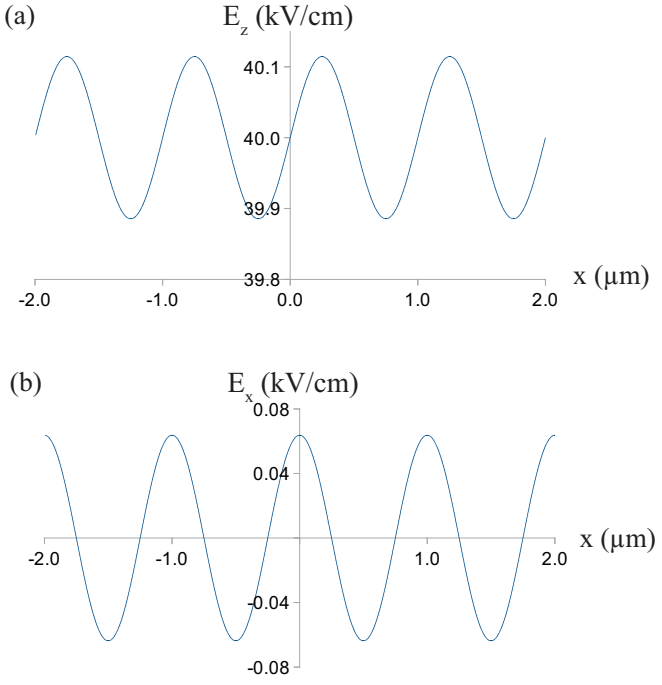

FIG. 9. Coordinate dependence of the electric field in the QW plane. (a) Component normal to the QW plane. (b) In-plane component.

TABLE IV. Parameters used to solve the 1D Schrödinger equation along z: the exciton effective mass m, the in-plane electron mass m_e, the dielectric constant ε, the transversal effective masses for the electron (hole) in the QW m_e^w (m_h^w) and in the barrier m_e^b (m_h^b), the corresponding barrier potential magnitude U_e^0 and U_h^0 for GaAs-based structures, the tunneling barrier energy $U_e^0 - E_0^e$ ($U_h^0 - E_0^h$) for MoS_2/hBN structure, and the radiative lifetimes of an exciton $\tau_{\rm dir}$ in an electric field $\mathbf{E} = 0$ and an indirect exciton $\tau_{\rm bright}$ in the radiative zone for $\mathbf{E} = \{0,0,E_z^{\rm av}\}$.

Quantity	GaAs/ AlGaAs CQWs	GaAs/ AlGaAs SQW	MoS_2/ hBN CQWs
m/m_0	0.22	0.22	1
m_e/m_0	0.067	0.067	0.5
ε	12.5	12.5	6.7
m_e^w/m_0	0.067	0.067	0.5
m_e^b/m_0	0.067	0.067	0.5
m_h^w/m_0	0.4	0.4	0.5
m_h^w/m_0	0.4	0.4	0.5
U_e^0 (eV)	0.3	0.3	
U_h^0 (eV)	0.15	0.15	
$U_e^0 - E_0^e$ (eV)			3[a]
$U_h^0 - E_0^h$ (eV)			3[a]
$\tau_{\rm dir}$ (ps)	100[b]	200[c]	0.4[d]
$\tau_{\rm bright}$ (ns)	150	2	100

[a]Reference [60].
[b]Reference [13].
[c]Reference [10].
[d]Reference [139].

where $\psi_{e,h}(z)$ are electron (hole) ground-state wave functions which are satisfied by the following 1D Schrödinger equation:

$$\left(-\frac{\hbar^2}{2m_{e,h}^z}\frac{d^2}{dz^2} + U_{e,h}(z) \pm eE_z^{\rm av} z - E_0^{e,h}\right)\psi_{e,h}(z) = 0, \tag{A7}$$

and normalized according to $\int \psi_{e,h}^2(z)dz = 1$. In Eq. (A7) $e > 0$ is the absolute value of the particle charge ("+" is for electron and "−" for hole), the z axis is along the normal to the QW plane, $U_{e,h}(z)$ is the QW potential for the electron (hole), $m_{e(h)}^z$ and $E_0^{e(h)}$ are effective masses along the z axis and ground-state energies for electron (hole), respectively [138]. Parameters of the QW structures used to solve (A7) are given in Table IV.

Exciton lifetime τ is estimated to be $\tau \sim 50\,\tau_{\rm bright}$ for GaAs-based structures and $\tau \sim \tau_{\rm bright}$ for the MoS_2/hBN structure [140], as

$$\tau_{\rm bright} = M^2\tau_{\rm dir},\ M \equiv \int \psi_e(z)\psi_h(z)dz, \tag{A8}$$

where $\tau_{\rm dir}$ is the lifetime of a direct exciton in zero electric field.

Binding energy and average in-plane electron-hole separation are calculated as $E_B = -H(\Delta x_m)$ and $r_{\rm ex} = \Delta x_m$, respectively (see also variational calculation results [141]).

TABLE V. Parameters for the proposed method of the condensate acceleration: the in-plane magnetic field $B_\parallel$, the magnitude of the e-h separation change ΔD, and the resulting system velocity v.

Quantity	GaAs/ AlGaAs CQWs	GaAs/ AlGaAs SQW
$B_\parallel$ (T)	8	8
ΔD (nm)	0.5	1.5
v (cm/sec)	3.2×10^5	9.6×10^5
Excitons	dark	dark

Here [142]

$$H(\Delta x) = \frac{\hbar^2}{2m_r \Delta x^2} - \frac{e^2/\varepsilon}{\sqrt{D^2 + \Delta x^2}}, \tag{A9}$$

$m_r = m_e(m - m_e)/m$ is the reduced mass of e and h, and Δx_m corresponds to the minimum of function (A9).

We estimate the effective exciton diameter due to internal electron-hole structure as twice the average distance between the center of mass and the position of the lighter carrier:

$$a_{ex} = r_{ex}(1 + \sqrt{1 - 4m_r/m}). \tag{A10}$$

The exciton core diameter arising from dipole-dipole interactions between excitons is given by the s-wave scattering length. To improve the accuracy, we use an energy-dependent [143] s-wave scattering length [27]:

$$a_s^{dd} = a_s^a \exp\left(b_s^a \ln p + c_s^a \ln^2 p + d_s^a \ln^3 p\right), \tag{A11}$$

where $p \sim \sqrt{2E/N}$, $a_s^a = 0.68845$, $b_s^a = -0.45897$, $c_s^a = -0.03098$, and $d_s^a = 0.002096$. For the considered regime $a_{ex} \lessapprox a_s^{dd}$ (see Table VI) the real exciton diameter is given by a_s^{dd} rather than a_{ex}.

4. Acceleration of the condensate with electric field switching

We have calculated the estimates for the velocity acquired by excitons set into motion with the procedure described in Sec. IV. Results are presented in Table V. We note that the switching is fast enough to ignore the exciton recombination, but slow enough to be considered adiabatic and ignore the normal component.

(1) Exciton lifetime τ (see Table VI) is much larger than the switching time τ_{sw}. Consequently, exciton recombination does not affect the velocity of superfluid motion.

(2) On the other hand, τ_{sw} is much larger then τ_{dissip}^{norm}, the time of normal component dissipation [130]. Thus the normal component is approximately at rest during switching.

(3) In the contemporary experiments [6,37] on exciton BEC the characteristic size L of the system is on the order of 10–100 μm and is much smaller than $L_{max}^{adiab} \equiv \pi C_s \tau_{sw}$. It follows then that the switching process does not noticeably excite the system and thus can be considered as adiabatical.

APPENDIX B: ANALYSIS OF EXPERIMENTAL REALIZATION OF THE EFFECTS

Feasibility of the proposed experiments is supported by the data summarized in Table VI.

(1) C_s for the excitonic system is larger than the sound velocity c_{LA}^{phon} for longitudinal acoustic phonons in the QW material. This enables efficient cooling of excitons by semiconductor lattice through emission of "Cherenkov" phonons. Because of this excitons can cool down to temperatures as low as $T = 0.1$ K [6] during their lifetime. This temperature is evidently smaller than the estimate for superfluid crossover T_c.

(2) Binding energy of an exciton E_B is larger than the sum of the chemical potential μ and the dissociation energy due to an in-plane field $E_{dissoc}^{in-plane} = eE_x^0\lambda/\pi$. This means that the dissociation of an exciton by tunneling of e and h to neighboring nodes of the in-plane field $E_x(x) = E_x^0 \sin(2\pi x/\lambda)$ (which is most profitable energetically) is forbidden.

(3) Effective exciton diameter a_{ex} is close to (or smaller then) the energy-dependent s-wave scattering length a_s^{dd} due to the dipole-dipole interactions. It follows then that the overlap

TABLE VI. Parameters of the proposed realizations: the exciton lifetime τ, the switching time for the electric field (see Sec. IV) τ_{sw}, the normal component dissipation time τ_{dissip}^{norm}, the maximal system size for the electric field switching to be adiabatic L_{max}^{adiab}, the sound velocity in the exciton superfluid C_s (average value neglecting periodic potential), the sound velocity for longitudinal acoustic phonons in a semiconductor c_{LA}^{semic}, the dissociation energy by the in-plane field $E_{dissoc}^{in-plane}$, the average in-plane electron-hole separation r_{ex}, the effective exciton diameter a_{ex}, the energy-dependent s-wave scattering length due to dipolar interactions a_s^{dd}, the exciton binding energy E_B, and the maximal electric field for which the transition of spatially indirect excitons into direct ones is allowed $E_z^{ind-dir}$. Structures are the same as in Table I.

Quantity	GaAs/ AlGaAs/ GaAs CQWs	GaAs/ AlGaAs SQW	MoS_2/ hBN/ MoS_2 CQWs	$MoSe_2$/ hBN/ WSe2 CQWs
τ (μs)	> 6	> 0.1	> 0.1	> 0.1[a]
τ_{sw} (ns)	8	5		
τ_{dissip}^{norm} (ps)	10	10		
L_{max}^{adiab} (μm)	501	473		
C_s (10^5 cm/sec)	20	30	57	74
c_{LA}^{semic} (10^5 cm/sec)	5.36	5.36	7.11[b]	4.1[c]
$E_{dissoc}^{in-plane}$ (meV)	2.0	0.9	17	23
r_{ex} (nm)	22	26	2.1	2.3
a_{ex} (nm)	30.7	36.1	2.7	2.3
a_s^{dd} (nm)	30.0	34.3	3.7	2.2
E_B (meV)	2.8	2.4	43.1	50.6
$E_z^{ind-dir}$ (kV/cm)	7[d]	4[e]	~ 2000[f]	~ 2000[g]

[a]Reference [144].
[b]Reference [145].
[c]Reference [146].
[d]Reference [13].
[e]Reference [10].
[f]Reference [60].
[g]Reference [62].

between the wave functions of the neighboring excitons is not too large and the exchange effects can be neglected at least for qualitative purposes (i.e., fermionic effects are not too important and the excitons can be considered as bosons).

(4) In GaAs coupled QWs transformation of spatially indirect excitons into direct ones does not take place. The reason is that the maximal electric field $E_z^{\mathrm{ind-dir}}$ for which this is possible is smaller then the minimal value of E_z. In $MoSe_2$/hBN/WSe_2 QWs an exciton ground state corresponds to an indirect exciton. Therefore, since the maximal value of E_z is smaller than $E_z^{\mathrm{ind-dir}}$, the indirect-direct exciton transition is forbidden as well. In MoS_2/hBN/MoS_2 QWs, on the contrary, for the parameters considered this transition is allowed. The transition is nonresonant and must be accompanied by emission of a phonon. This gives an additional nonradiative channel of indirect exciton decay with characteristic time set by scattering on acoustic phonons. In the case we have considered it will be suppressed due to the relatively large interwell distance.

(5) According to the results of our calculation in the MoS_2/hBN QW for electron-hole separation $D = 2$ nm, $E_z^{\mathrm{av}} = 256$ kV/cm compensates the z component of $eE_z^{eh}(D) = d[\mu(z) - E_B(z)]/dz|_{z=D}$; the electron-hole attraction in an indirect exciton. In this case disorder caused by fluctuations of hBN barrier width is suppressed which is important for superfluid properties [91]. For $MoSe_2$/hBN/WSe_2 QWs, which have $D = 1.333$ nm, the field $E_z^{\mathrm{av}} = 447$ kV/cm also corresponds to compensation.

[1] V. L. Berezinskii, Sov. Phys. JETP **32**, 493 (1970); **34**, 610 (1971); J. M. Kosterlitz and D. J. Thouless, J. Phys. C **6**, 1181 (1973); J. M. Kosterlitz, *ibid.* **7**, 1046 (1974); D. R. Nelson and J. M. Kosterlitz, Phys. Rev. Lett. **39**, 1201 (1977).

[2] K. B. Davis, M. O. Mewes, M. R. Andrews, N. J. van Druten, D. S. Durfee, D. M. Kurn, and W. Ketterle, Phys. Rev. Lett. **75**, 3969 (1995); M. H. Anderson, J. R. Ensher, M. R. Matthews, C. E. Wieman, and E. A. Cornell, Science **269**, 198 (1995).

[3] M. W. Zwierlein, C. A. Stan, C. H. Schunck, S. M. F. Raupach, S. Gupta, Z. Hadzibabic, and W. Ketterle, Phys. Rev. Lett. **91**, 250401 (2003).

[4] Z. Hadzibabic, P. Krüger, M. Cheneau, B. Battelier, and J. Dalibard, Nature (London) **441**, 1118 (2006).

[5] L. Pitaevskii and S. Stringari, *Bose-Einstein Condensation* (Clarendon, Oxford, 2013).

[6] A. A. High, J. R. Leonard, A. T. Hammack, M. M. Fogler, L. V. Butov, A. V. Kavokin, K. L. Campman, and A. C. Gossard, Nature (London) **483**, 584 (2012); A. A. High, J. R. Leonard, M. Remeika, L. V. Butov, M. Hanson, and A. C. Gossard, Nano Lett. **12**, 2605 (2012); A. A. High, A. T. Hammack, J. R. Leonard, S. Yang, L. V. Butov, T. Ostatnický, M. Vladimirova, A. V. Kavokin, T. C. H. Liew, K. L. Campman, and A. C. Gossard, Phys. Rev. Lett. **110**, 246403 (2013).

[7] J. Kasprzak, M. Richard, S. Kundermann, A. Baas, P. Jeambrun, J. M. J. Keeling, F. M. Marchetti, M. H. Szymańska, R. André, J. L. Staehli, V. Savona, P. B. Littlewood, B. Deveaud, and Le Si Dang, Nature (London) **443**, 409 (2006).

[8] Yu. E. Lozovik and V. I. Yudson, JETP Lett. **22**, 274 (1975); Sov. Phys. JETP **44**, 389 (1976); Solid State Commun. **19**, 391 (1976); **21**, 211 (1977); **22**, 117 (1977).

[9] L. V. Butov, J. Phys.: Condens. Matter **16**, R1577 (2004); V. B. Timofeev, A. V. Gorbunov, and A. V. Larionov, *ibid.* **19**, 295209 (2007); R. Rapaport and G. Chen, *ibid.* **19**, 295207 (2007); M. Combescot, O. Betbeder-Matibet, and F. Dubin, Phys. Rep. **463**, 215 (2008); D. W. Snoke, Adv. Condens. Matter Phys. **2011**, 938609 (2011); L. V. Butov, JETP **122**, 434 (2016).

[10] V. V. Solov'ev, I. V. Kukushkin, J. Smet, K. von Klitzing, and W. Dietsche, JETP Lett. **83**, 553 (2006); **84**, 222 (2006).

[11] A. Filinov, P. Ludwig, Yu. E. Lozovik, M. Bonitz, and H. Stolz, J. Phys.: Conf. Ser. **35**, 197 (2006); P. Ludwig, A. Filinov, M. Bonitz, and H. Stolz, Phys. Status Solidi B **243**, 2363 (2006); K. Sperlich, P. Ludwig, A. Filinov, M. Bonitz, H. Stolz, D. Hommel, and A. Gust, Phys. Status Solidi C **6**, 551 (2009).

[12] T. C. Damen, J. Shah, D. Y. Oberli, D. S. Chemla, J. E. Cunningham, and J. M. Kuo, Phys. Rev. B **42**, 7434 (1990).

[13] L. V. Butov, A. Imamoglu, A. V. Mintsev, K. L. Campman, and A. C. Gossard, Phys. Rev. B **59**, 1625 (1999).

[14] L. V. Butov, A. L. Ivanov, A. Imamoglu, P. B. Littlewood, A. A. Shashkin, V. T. Dolgopolov, K. L. Campman, and A. C. Gossard, Phys. Rev. Lett. **86**, 5608 (2001).

[15] C. Piermarocchi, F. Tassone, V. Savona, A. Quattropani, and P. Schwendimann, Phys. Rev. B **53**, 15834 (1996).

[16] A. G. Winbow, A. T. Hammack, L. V. Butov, and A. C. Gossard, Nano Lett. **7**, 1349 (2007).

[17] O. L. Berman, Yu. E. Lozovik, D. W. Snoke, and R. D. Coalson, Phys. Rev. B **70**, 235310 (2004); **73**, 235352 (2006); Solid State Commun. **134**, 47 (2005); Physica E **34**, 268 (2006); J. Phys.: Condens. Matter **19**, 386219 (2007).

[18] Yu. E. Lozovik and A. M. Ruvinskii, JETP **87**, 788 (1998); Yu. E. Lozovik, O. L. Berman, and A. M. Ruvinsky, JETP Lett. **69**, 616 (1999); Yu. E. Lozovik and M. Willander, Appl. Phys. A **71**, 379 (2000).

[19] V. M. Kovalev and A. V. Chaplik, JETP Lett. **92**, 185 (2010); M. Alloing, A. Lemaître, and F. Dubin, Europhys. Lett. **93**, 17007 (2011).

[20] V. Srinivas, J. Hryniewicz, Y. J. Chen, and C. E. C. Wood, Phys. Rev. B **46**, 10193 (1992).

[21] C. Schindler and R. Zimmermann, Phys. Rev. B **78**, 045313 (2008).

[22] M. Combescot, O. Betbeder-Matibet, and R. Combescot, Phys. Rev. Lett. **99**, 176403 (2007).

[23] A. Filinov, M. Bonitz, P. Ludwig, and Yu. E. Lozovik, Phys. Status Solidi C **3**, 2457 (2006).

[24] A. A. Dremin, V. B. Timofeev, A. V. Larionov, J. Hvam, and C. Soerensen, JETP Lett. **76**, 450 (2002).

[25] R. Maezono, P. López Ríos, T. Ogawa, and R. J. Needs, Phys. Rev. Lett. **110**, 216407 (2013).

[26] Yu. E. Lozovik, O. L. Berman, and V. G. Tsvetus, JETP Lett. **66**, 355 (1997).

[27] Yu. E. Lozovik, I. L. Kurbakov, G. E. Astrakharchik, and M. Willander, JETP **106**, 296 (2008).

[28] M. V. Kochiev, V. A. Tsvetkov, and N. N. Sibeldin, JETP Lett. **95**, 481 (2012); M. D. Fraser, H. H. Tan, and C. Jagadish, Phys. Rev. B **84**, 245318 (2011).
[29] A. V. Gorbunov and V. B. Timofeev, JETP Lett. **84**, 329 (2006); V. B. Timofeev and A. V. Gorbunov, J. Appl. Phys. **101**, 081708 (2007); Phys. Status Solidi C **5**, 2379 (2008); J. Phys.: Conf. Ser. **148**, 012049 (2009).
[30] P. Pieri, D. Neilson, and G. C. Strinati, Phys. Rev. B **75**, 113301 (2007).
[31] A. T. Hammack, M. Griswold, L. V. Butov, L. E. Smallwood, A. L. Ivanov, and A. C. Gossard, Phys. Rev. Lett. **96**, 227402 (2006).
[32] G. J. Schinner, E. Schubert, M. P. Stallhofer, J. P. Kotthaus, D. Schuh, A. K. Rai, D. Reuter, A. D. Wieck, and A. O. Govorov, Phys. Rev. B **83**, 165308 (2011).
[33] A. V. Gorbunov and V. B. Timofeev, JETP Lett. **96**, 138 (2012).
[34] A. A. High, A. K. Thomas, G. Grosso, M. Remeika, A. T. Hammack, A. D. Meyertholen, M. M. Fogler, L. V. Butov, M. Hanson, and A. C. Gossard, Phys. Rev. Lett. **103**, 087403 (2009).
[35] W. Zhao, P. Stenius, and A. Imamoglu, Phys. Rev. B **56**, 5306 (1997); M. H. Szymanska, J. Keeling, and P. B. Littlewood, Phys. Rev. Lett. **96**, 230602 (2006).
[36] S. Yang, A. T. Hammack, M. M. Fogler, L. V. Butov, and A. C. Gossard, Phys. Rev. Lett. **97**, 187402 (2006).
[37] Y. Shilo, K. Cohen, B. Laikhtman, K. West, L. Pfeiffer, and R. Rapaport, Nat. Commun. **4**, 2335 (2013); M. Stern, V. Umansky, and I. Bar-Joseph, Science **343**, 55 (2014); M. Alloing, M. Beian, D. Fuster, Y. Gonzalez, L. Gonzalez, R. Combescot, M. Combescot, and F. Dubin, Europhys. Lett. **107**, 10012 (2014); S. Yang, L. V. Butov, B. D. Simons, K. L. Campman, and A. C. Gossard, Phys. Rev. B **91**, 245302 (2015).
[38] K. I. Golden, G. J. Kalman, P. Hartmann, and Z. Donko, Phys. Rev. E **82**, 036402 (2010); Y. G. Rubo and A. V. Kavokin, Phys. Rev. B **84**, 045309 (2011); A. V. Kavokin, M. Vladimirova, B. Jouault, T. C. H. Liew, J. R. Leonard, and L. V. Butov, *ibid.* **88**, 195309 (2013); D. Neilson, A. Perali, and A. R. Hamilton, *ibid.* **89**, 060502 (2014); S. V. Andreev, A. A. Varlamov, and A. V. Kavokin, Phys. Rev. Lett. **112**, 036401 (2014); M. Combescot, R. Combescot, M. Alloing, and F. Dubin, *ibid.* **114**, 090401 (2015); F.-C. Wu, F. Xue, and A. H. MacDonald, Phys. Rev. B **92**, 165121 (2015).
[39] A. V. Klyuchnik and Yu. E. Lozovik, J. Phys. C **11**, L483 (1978).
[40] Yu. E. Lozovik and A. V. Poushnov, Phys. Lett. A **228**, 399 (1997).
[41] A. K. Fedorov, I. L. Kurbakov, and Yu. E. Lozovik, Phys. Rev. B **90**, 165430 (2014).
[42] S. V. Andreev, Phys. Rev. Lett. **110**, 146401 (2013); Phys. Rev. B **92**, 041117 (2015).
[43] Yu. E. Lozovik, S. Yu. Volkov, and M. Willander, JETP Lett. **79**, 473 (2004).
[44] I. L. Kurbakov, Yu. E. Lozovik, G. E. Astrakharchik, and J. Boronat, Phys. Rev. B **82**, 014508 (2010); J. Ye, J. Low Temp. Phys. **158**, 882 (2010); M. Matuszewski, T. Taylor, and A. V. Kavokin, Phys. Rev. Lett. **108**, 060401 (2012).
[45] A thermodynamically stable supersolid state can be realized when roton-like attraction [41] and many-body repulsion [147] coexist; see Z.-K. Lu, Y. Li, D. S. Petrov, and G. V. Shlyapnikov, Phys. Rev. Lett. **115**, 075303 (2015).
[46] A. Filinov, N. V. Prokof'ev, and M. Bonitz, Phys. Rev. Lett. **105**, 070401 (2010).
[47] Yu. E. Lozovik, I. L. Kurbakov, and M. Willander, Phys. Lett. A **366**, 487 (2007).
[48] E. B. Sonin, Phys. Rev. Lett. **102**, 106407 (2009); S. I. Shevchenko, Phys. Rev. B **56**, 10355 (1997).
[49] J. Keeling, L. S. Levitov, and P. B. Littlewood, Phys. Rev. Lett. **92**, 176402 (2004); J. Ye, T. Shi, and L. Jiang, *ibid.* **103**, 177401 (2009).
[50] Yu. E. Lozovik, I. L. Kurbakov, and I. V. Ovchinnikov, Solid State Commun. **126**, 269 (2003).
[51] C.-E. Bardyn, T. Karzig, G. Refael, and T. C. H. Liew, Phys. Rev. B **91**, 161413 (2015).
[52] Q.-D. Jiang, Z.-Q. Bao, Q.-F. Sun, and X. C. Xie, Sci. Rep. **5**, 11925 (2015).
[53] T. Hakioğlu, E. Özgün, and M. Günay, Appl. Phys. Lett. **104**, 162105 (2014).
[54] R. Anankine, M. Beian, S. Dang, M. Alloing, E. Cambril, K. Merghem, C. G. Carbonell, A. Lemaitre, and F. Dubin, Phys. Rev. Lett. **118**, 127402 (2017).
[55] J. P. Eisenstein and A. H. MacDonald, Nature (London) **432**, 691 (2004).
[56] A. Perali, D. Neilson, and A. R. Hamilton, Phys. Rev. Lett. **110**, 146803 (2013); D. S. L. Abergel, M. Rodriguez-Vega, E. Rossi, and S. Das Sarma, Phys. Rev. B **88**, 235402 (2013).
[57] O. L. Berman, R. Ya. Kezerashvili, and K. Ziegler, Phys. Rev. B **85**, 035418 (2012).
[58] D. K. Efimkin, Yu. E. Lozovik, and A. A. Sokolik, Phys. Rev. B **86**, 115436 (2012).
[59] L. V. Kulik, A. V. Gorbunov, A. S. Zhuravlev, V. B. Timofeev, S. Dickmann, and I. V. Kukushkin, Sci. Rep. **5**, 10354 (2015).
[60] M. M. Fogler, L. V. Butov, and K. S. Novoselov, Nat. Commun. **5**, 4555 (2014); E. V. Calman, C. J. Dorow, M. M. Fogler, L. V. Butov, S. Hu, A. Mishchenko, and A. K. Geim, Appl. Phys. Lett. **108**, 101901 (2016).
[61] K. F. Mak, C. Lee, J. Hone, J. Shan, and T. F. Heinz, Phys. Rev. Lett. **105**, 136805 (2010); A. K. Geim and I. V. Grigorieva, Nature (London) **499**, 419 (2013).
[62] P. Rivera, J. R. Schaibley, A. M. Jones, J. S. Ross, S. F. Wu, G. Aivazian, P. Klement, K. Seyler, G. Clark, N. J. Ghimire, J. Q. Yan, D. G. Mandrus, W. Yao, and X. D. Xu, Nat. Commun. **6**, 6242 (2015).
[63] P. Rivera, K. L. Seyler, H. Y. Yu, J. R. Schaibley, J. Q. Yan, D. G. Mandrus, W. Yao, and X. D. Xu, Science **351**, 688 (2016).
[64] T. Cheiwchanchamnangij and W. R. L. Lambrecht, Phys. Rev. B **85**, 205302 (2012); S. F. Wu, J. S. Ross, G.-B. Liu, G. Aivazian, A. Jones, Z. Y. Fei, W. G. Zhu, D. Xiao, W. Yao, D. Cobden, and X. D. Xu, Nat. Phys. **9**, 149 (2013).
[65] A. T. Hammack, N. A. Gippius, S. Yang, G. O. Andreev, L. V. Butov, M. Hanson, and A. C. Gossard, J. Appl. Phys. **99**, 066104 (2006).
[66] Y. Y. Kuznetsova, A. A. High, and L. V. Butov, Appl. Phys. Lett. **97**, 201106 (2010).
[67] Z. Vörös, D. W. Snoke, L. Pfeiffer, and K. West, Phys. Rev. Lett. **97**, 016803 (2006); K. Kowalik-Seidl, X. P. Vögele, F. Seilmeier, D. Schuh, W. Wegscheider, A. W. Holleitner, and

J. P. Kotthaus, Phys. Rev. B **83**, 081307 (2011); M. Alloing, A. Lemaître, E. Galopin, and F. Dubin, Sci. Rep. **3**, 1578 (2013).
[68] G. Chen, R. Rapaport, L. N. Pffeifer, K. West, P. M. Platzman, S. Simon, Z. Vörös, and D. Snoke, Phys. Rev. B **74**, 045309 (2006); K. Kowalik-Seidl, X. P. Vögele, B. N. Rimpfl, G. J. Schinner, D. Schuh, W. Wegscheider, A. W. Holleitner, and J. P. Kotthaus, Nano Lett. **12**, 326 (2012).
[69] Z. Vörös, D. W. Snoke, L. Pfeiffer, and K. West, Phys. Rev. Lett. **103**, 016403 (2009).
[70] M. Remeika, J. C. Graves, A. T. Hammack, A. D. Meyertholen, M. M. Fogler, L. V. Butov, M. Hanson, and A. C. Gossard, Phys. Rev. Lett. **102**, 186803 (2009); M. Remeika, J. R. Leonard, C. J. Dorow, M. M. Fogler, L. V. Butov, M. Hanson, and A. C. Gossard, Phys. Rev. B **92**, 115311 (2015).
[71] M. Remeika, M. M. Fogler, L. V. Butov, M. Hanson, and A. C. Gossard, Appl. Phys. Lett. **100**, 061103 (2012).
[72] A. Abdelrahman and B. S. Ham, Phys. Rev. B **86**, 085445 (2012); **87**, 125311 (2013).
[73] A. G. Winbow, J. R. Leonard, M. Remeika, Y. Y. Kuznetsova, A. A. High, A. T. Hammack, L. V. Butov, J. Wilkes, A. A. Guenther, A. L. Ivanov, M. Hanson, and A. C. Gossard, Phys. Rev. Lett. **106**, 196806 (2011).
[74] A. A. High, A. T. Hammack, L. V. Butov, M. Hanson, and A. C. Gossard, Opt. Lett. **32**, 2466 (2007).
[75] J. Krauss, J. P. Kotthaus, A. Wixforth, M. Hanson, D. C. Driscoll, A. C. Gossard, D. Schuh, and M. Bichler, Appl. Phys. Lett. **85**, 5830 (2004).
[76] M. W. Hasling, Y. Y. Kuznetsova, P. Andreakou, J. R. Leonard, E. V. Calman, C. J. Dorow, L. V. Butov, M. Hanson, and A. C. Gossard, J. Appl. Phys. **117**, 023108 (2015).
[77] Y. Y. Kuznetsova, P. Andreakou, M. W. Hasling, J. R. Leonard, E. V. Calman, L. V. Butov, M. Hanson, and A. C. Gossard, Opt. Lett. **40**, 589 (2015).
[78] J. R. Leonard, M. Remeika, M. K. Chu, Y. Y. Kuznetsova, A. A. High, L. V. Butov, J. Wilkes, M. Hanson, and A. C. Gossard, Appl. Phys. Lett. **100**, 231106 (2012); P. Andreakou, S. V. Poltavtsev, J. R. Leonard, E. V. Calman, M. Remeika, Y. Y. Kuznetsova, L. V. Butov, J. Wilkes, M. Hanson, and A. C. Gossard, *ibid.* **104**, 091101 (2014); C. J. Dorow, Y. Y. Kuznetsova, J. R. Leonard, M. K. Chu, L. V. Butov, J. Wilkes, M. Hanson, and A. C. Gossard, *ibid.* **108**, 073502 (2016).
[79] J. Rudolph, R. Hey, and P. V. Santos, Phys. Rev. Lett. **99**, 047602 (2007); S. Lazić, A. Violante, K. Cohen, R. Hey, R. Rapaport, and P. V. Santos, Phys. Rev. B **89**, 085313 (2014).
[80] E. A. Cerda-Méndez, D. N. Krizhanovskii, M. Wouters, R. Bradley, K. Biermann, K. Guda, R. Hey, P. V. Santos, D. Sarkar, and M. S. Skolnick, Phys. Rev. Lett. **105**, 116402 (2010).
[81] S. Müller, J. Billy, E. A. L. Henn, H. Kadau, A. Griesmaier, M. Jona-Lasinio, L. Santos, and T. Pfau, Phys. Rev. A **84**, 053601 (2011).
[82] N. Fabbri, D. Clément, L. Fallani, C. Fort, M. Modugno, K. M. R. van der Stam, and M. Inguscio, Phys. Rev. A **79**, 043623 (2009).
[83] L.-C. Ha, L. W. Clark, C. V. Parker, B. M. Anderson, and C. Chin, Phys. Rev. Lett. **114**, 055301 (2015).
[84] P. T. Ernst, S. Götze, J. S. Krauser, K. Pyka, D.-S. Lühmann, D. Pfannkuche, and K. Sengstock, Nat. Phys. **6**, 56 (2009).
[85] M. Krämer, C. Menotti, L. Pitaevskii, and S. Stringari, Eur. Phys. J. D **27**, 247 (2003).
[86] K. Berg-Sørensen and K. Mølmer, Phys. Rev. A **58**, 1480 (1998).
[87] K. Góral, L. Santos, and M. Lewenstein, Phys. Rev. Lett. **88**, 170406 (2002); H. P. Büchler and G. Blatter, *ibid.* **91**, 130404 (2003); C. Trefzger, C. Menotti, and M. Lewenstein, *ibid.* **103**, 035304 (2009); I. Danshita and C. A. R. Sá de Melo, *ibid.* **103**, 225301 (2009).
[88] R. M. Wilson and J. L. Bohn, Phys. Rev. A **83**, 023623 (2011).
[89] J. Javanainen, Phys. Rev. A **60**, 4902 (1999); M. Krämer, L. Pitaevskii, and S. Stringari, Phys. Rev. Lett. **88**, 180404 (2002).
[90] K. Huang and H.-F. Meng, Phys. Rev. Lett. **69**, 644 (1992).
[91] S. Giorgini, L. Pitaevskii, and S. Stringari, Phys. Rev. B **49**, 12938 (1994).
[92] O. Penrose and L. Onsager, Phys. Rev. **104**, 576 (1956).
[93] A. J. Leggett, Rev. Mod. Phys. **47**, 331 (1975).
[94] G. E. Volovik, Superfluid He3: Hydrodynamics and inhomogeneous states, in *Soviet Scientific Reviews, Section A: Physics Reviews*, edited by I. M. Khalatnikov (Harwood, London, 1979), p. 23.
[95] V. P. Mineev, Nat. Phys. **8**, 253 (2012).
[96] J.-S. You, H. Lee, S. Fang, M. A. Cazalilla, and D.-W. Wang, Phys. Rev. A **86**, 043612 (2012).
[97] M. Iskin and C. A. R. Sá de Melo, Phys. Rev. Lett. **103**, 165301 (2009).
[98] D. Chowdhury, E. Berg, and S. Sachdev, Phys. Rev. B **84**, 205113 (2011).
[99] A. Macia, F. Mazzanti, J. Boronat, and R. E. Zillich, Phys. Rev. A **84**, 033625 (2011).
[100] C. Ticknor, Phys. Rev. A **86**, 053602 (2012).
[101] J. Schönmeier-Kromer and L. Pollet, Phys. Rev. A **89**, 023605 (2014).
[102] P. Minnhagen and P. Olsson, Phys. Rev. B **44**, 4503 (1991).
[103] P. Muruganandam and S. K. Adhikari, Phys. Lett. A **376**, 480 (2012); G. Bismut, B. Laburthe-Tolra, E. Marechal, P. Pedri, O. Gorceix, and L. Vernac, Phys. Rev. Lett. **109**, 155302 (2012).
[104] C. Ticknor, R. M. Wilson, and J. L. Bohn, Phys. Rev. Lett. **106**, 065301 (2011).
[105] D. M. Stamper-Kurn, New J. Phys. **5**, 50 (2003).
[106] B. C. Mulkerin, R. M. W. van Bijnen, D. H. J. O'Dell, A. M. Martin, and N. G. Parker, Phys. Rev. Lett. **111**, 170402 (2013).
[107] X.-F. Zhang, L. Wen, C.-Q. Dai, R.-F. Dong, H.-F. Jiang, H. Chang, and S.-G. Zhang, Sci. Rep. **6**, 19380 (2016).
[108] M. E. Fisher, M. N. Barber, and D. Jasnow, Phys. Rev. A **8**, 1111 (1973).
[109] The strong-correlation mode ($[N - N_0]/N \sim 1$) is frequently realized for two-dimensional excitons [124]. However, we present only the solution for weak correlations because it allows one to obtain general formulas in an analytical form. We assume that the qualitative conclusions we obtain can be applied to strongly correlated systems.
[110] For strictly bosonic excitons spin degrees of freedom are manifest only in the splitting (Zeeman, exchange, etc.) of the excitonic band bottom. One can show by a straightforward calculation using the Gross-Pitaevskii equation that in the weak correlation and modulation regime the condensate populates only the lowest in energy spin degree of freedom. The condensate spin basis coincides then with the single-exciton spin basis allowing one to consider the problem assuming a single spin band.
[111] Yu. E. Lozovik and V. I. Yudson, Physica A **93**, 493 (1978).

[112] The finiteness of (18) means that (18) will be sufficiently small for weak potentials U and V_0, which means that $n_0 = n - n'$ will certainly be positive.

[113] Notice that expressions for $n - n_0$ and $\langle \hat{H}' \rangle$ are invariant under $\mathbf{q} \leftrightarrow -\mathbf{q}$. For quantities carrying $+/-$ indices (except $f_\pm$) this operation as can be seen from (14) is equivalent to simply $+ \leftrightarrow -$. In the expressions for observables there are only two vector quantities: $\mathbf{P}$ and $\mathbf{q}$. $\mathbf{P}$ enters all the expressions except for the spectrum (17) in the form of α. However, because in (17) $\mathbf{P}$ forms a product with the integration variable (for energy) the answer will contain the product with some other vector. All the other $\mathbf{P}$ are part of α so it means that in the final answer $\mathbf{P}$ will come in α. $\mathbf{q}$ in the answer can be in the form of $\mathbf{q}^2$ or α. Let us decompose the answer in α (remember that $\mathbf{P}$ is infinitesimal). Coefficients going with α in odd powers should be zero because the answer is symmetric under $\mathbf{q} \leftrightarrow -\mathbf{q}$. In the vicinity of $\mathbf{P} = 0$ this leads to (20).

[114] To make quantitative estimates we have used (25) and (26), but not (22). This allows one to avoid ambiguity between (24) and (22), which differ due to a neglected $O(\Delta_s^2)$ term in the first expression.

[115] A. Alexandrou, J. A. Kash, E. E. Mendez, M. Zachau, J. M. Hong, T. Fukuzawa, and Y. Hase, Phys. Rev. B **42**, 9225 (1990).

[116] R. Rapaport, G. Chen, S. Simon, O. Mitrofanov, L. Pfeiffer, and P. M. Platzman, Phys. Rev. B **72**, 075428 (2005).

[117] J. W. Kane and L. P. Kadanoff, Phys. Rev. **155**, 80 (1967).

[118] V. N. Popov, *Functional Integrals in Quantum Field Theory and Statistical Physics* (D. Reidel, Dordrecht, 1983).

[119] H.-F. Meng, Phys. Rev. B **49**, 1205 (1994). A brief overview of the hydrodynamic field theory calculation of the density matrix is given in [27] for uniform 2D systems at $T = 0$. A more detailed account is presented for the 1D case in D. L. Luxat and A. Griffin, Phys. Rev. A **67**, 043603 (2003).

[120] Expression (28) is valid for the case of a direct optical transition and applying rescaling [96,102] $x \to x/\eta$, $y \to \eta y$, where $\eta = [(\mathrm{Y}_s)_{xx}/(\mathrm{Y}_s)_{yy}]^{1/4}$, to the long-wavelength density matrix asymptotics [117] $\rho_1(r) \propto r^{-\alpha}$.

[121] In 2D a quasicondensate at $T = 0$ becomes a usual BEC [117]. Anisotropy of the angle-resolved luminescence of a BEC is determined by the geometrical form of the order parameter and is not connected to the superfluidity anisotropy.

[122] L. V. Butov, A. V. Mintsev, Yu. E. Lozovik, K. L. Campman, and A. C. Gossard, Phys. Rev. B **62**, 1548 (2000).

[123] L. V. Butov, C. W. Lai, D. S. Chemla, Yu. E. Lozovik, K. L. Campman, and A. C. Gossard, Phys. Rev. Lett. **87**, 216804 (2001).

[124] Yu. E. Lozovik, I. L. Kurbakov, G. E. Astrakharchik, J. Boronat, and M. Willander, Solid State Commun. **144**, 399 (2007).

[125] M. R. Andrews, D. M. Kurn, H.-J. Miesner, D. S. Durfee, C. G. Townsend, S. Inouye, and W. Ketterle, Phys. Rev. Lett. **79**, 553 (1997); **80**, 2967 (1998).

[126] Z. Vörös, R. Balili, D. W. Snoke, L. Pfeiffer, and K. West, Phys. Rev. Lett. **94**, 226401 (2005).

[127] C. Ciuti, V. Savona, C. Piermarocchi, A. Quattropani, and P. Schwendimann, Phys. Rev. B **58**, 7926 (1998).

[128] J. Lee, E. S. Koteles, and M. O. Vassell, Phys. Rev. B **33**, 5512 (1986); R. K. Basu and P. Ray, *ibid.* **45**, 1907 (1992).

[129] Strictly speaking, in the regime of the spatially resolved cw pump a finite exciton recombination rate already yields a nonzero motion velocity in the form of a continuous inflow to the studied area of the QW. We neglect this effect in (32) assuming the lifetime to be large enough.

[130] $\tau_{\mathrm{dissip}}^{\mathrm{norm}}$ can be estimated as the inverse damping rate of elementary excitations due to disorder. This rate has been found in [17] to be greater than 0.1 meV/$\hbar$; thus $\tau_{\mathrm{dissip}}^{\mathrm{norm}} \lesssim 10$ ps.

[131] A. G. Winbow, L. V. Butov, and A. C. Gossard, J. Appl. Phys. **104**, 063515 (2008).

[132] H. Shi, G. Verechaka, and A. Griffin, Phys. Rev. B **50**, 1119 (1994).

[133] K. W. Madison, F. Chevy, W. Wohlleben, and J. Dalibard, Phys. Rev. Lett. **84**, 806 (2000).

[134] A. V. Gorbunov, V. B. Timofeev, and D. A. Demin, JETP Lett. **94**, 800 (2012).

[135] G. E. Astrakharchik, J. Boronat, I. L. Kurbakov, and Yu. E. Lozovik, Phys. Rev. Lett. **98**, 060405 (2007).

[136] The BKT transition temperature in an anisotropic superfluid has the form [1] $T_c \approx \pi\hbar^2 n_s/2m$, where [96] $n_s/m = \sqrt{(\mathrm{Y}_s)_{xx}(\mathrm{Y}_s)_{yy}}$, and $(\mathrm{Y}_s)_{xx}$, $(\mathrm{Y}_s)_{yy}$ are the diagonal elements of the helicity modulus tensor. Taking $n \approx n_0$ into account one obtains from (25) $n_s = n_0\sqrt{1 - 2\Delta_s}$.

[137] When an incompressible nondissipatively moving liquid flows into a narrow channel, Bernoulli's law can lead to arbitrary high velocities even if outside the channel flow velocity is small. Thus the flow velocity in the channel can reach Landau critical velocity or higher values. The flow through the channel can be created by, e.g., pumping the excitons only on one side of the channel, while on the other they will only recombine.

[138] Because E_z^{av} is sufficiently weak (see Table III), we neglect the tunneling electron (hole) out of the QW.

[139] S. Sim, J. Park, J.-G. Song, C. In, Y.-S. Lee, H. Kim, and H. Choi, Phys. Rev. B **88**, 075434 (2013).

[140] For the MoS_2/hBN structure, we assume that the in-plane magnetic field is absent (see Sec. V). Therefore, the bottom of the excitonic dispersion is inside the radiative zone such that $\tau \sim \tau_{\mathrm{bright}}$. However, for GaAs-based structures the necessary in-plane magnetic field $B_\parallel = 8$ T (see Table V) is so large that the bottom of excitonic dispersion is far out of the radiative zone. Thus for moderate densities and sufficiently low temperatures the *ab initio* modeling [124] yields an occupation of the radiative zone so low that the main recombination channel is nonradiative (with momentum transfer to an additional particle). The exciton lifetime with respect to this channel is proportional [148] to M^2 and [132] τ_{dir}, i.e., $\tau \propto \tau_{\mathrm{bright}}$ [see (A8)]. A lower bound for the nonradiative exciton recombination time in the limit of strong in-plane magnetic fields is [149] $\tau \sim 50\,\tau_{\mathrm{bright}}$.

[141] Yu. E. Lozovik and V. N. Nishanov, Fiz. Tverd. Tela **18**, 3267 (1976).

[142] Here we employ uncertainty relation $\Delta p \sim \hbar/\Delta x$. The ground state energy of an exciton in an e-h bilayer is given by (A9). Minimizing (A9) with respect to Δx, we obtain the estimate $r_{\mathrm{ex}} = \Delta x_m$ for exciton radius and $E_B = -H(\Delta x_m)$ for exciton binding energy.

[143] G. E. Astrakharchik, J. Boronat, I. L. Kurbakov, Yu. E. Lozovik, and F. Mazzanti, Phys. Rev. A **81**, 013612 (2010).

[144] Unlike the MoS_2/hBN/MoS_2 structure, $MoSe_2$/hBN/WSe_2 is a type II QW. In this case the results of the tunneling model used in Appendix A 3 do not agree well with the experimental data [63]. To estimate τ for $MoSe_2$/hBN/WSe_2 CQWs we

use instead a crude estimate based on the experiment of L. Britnell, R. V. Gorbachev, R. Jalil, B. D. Belle, F. Schedin, A. Mishchenko, T. Georgiou, M. I. Katsnelson, L. Eaves, S. V. Morozov, N. M. R. Peres, J. Leist, A. K. Geim, K. S. Novoselov, and L. A. Ponomarenko, Science **335**, 947 (2012). For a nonresonant tunneling process this estimate yields τ 6 orders of magnitude larger than for a zero thickness hBN barrier (2 orders of magnitude per hBN monolayer). Thus at least $\tau > 0.1\mu$s.

[145] S. Ge, X. Liu, X. Qiao, Q. Wang, Z. Xu, J. Qiu, P. Tan, J. Zhao, and D. Sun, Sci. Rep. **4**, 5722 (2014).

[146] Z. Jin, Xiaodong Li, J. T. Mullen, and Ki Wook Kim, Phys. Rev. B **90**, 045422 (2014).

[147] B. Laikhtman and R. Rapaport, Phys. Rev. B **80**, 195313 (2009); G. J. Schinner, J. Repp, E. Schubert, A. K. Rai, D. Reuter, A. D. Wieck, A. O. Govorov, A. W. Holleitner, and J. P. Kotthaus, *ibid.* **87**, 205302 (2013).

[148] R. Ferreira and G. Bastard, Phys. Rev. B **40**, 1074 (1989).

[149] A. Parlangeli, P. C. M. Christianen, J. C. Maan, I. V. Tokatly, C. B. Soerensen, and P. E. Lindelof, Phys. Rev. B **62**, 15323 (2000).